AD-A112 089 PENNSYLVANIA STATE UNIV UNIVERSITY PARK APPLIED RESE--ETC F/G 20/4
A SPLINE SOLUTION OF THE INCOMPRESSIBLE PARABOLIZED NAVIER-STOK--ETC(U)
JAN 82 G H HOFFMAN N00024-79-C-6043
UNCLASSIFIED ARL/PSU/TM-82-51 NL

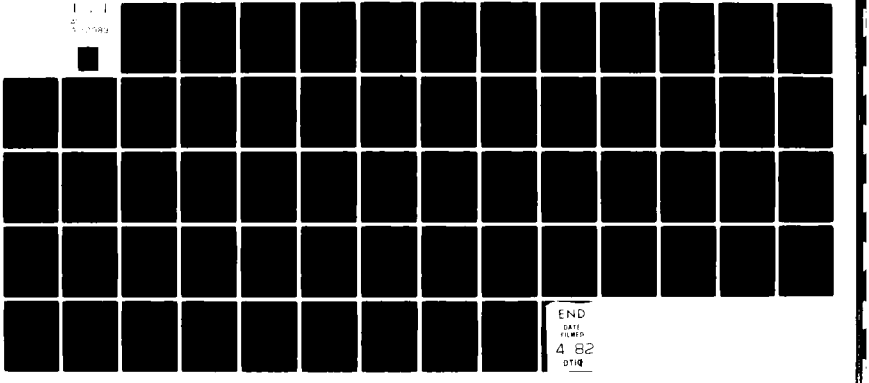

END
DATE FILMED
4 82
DTIC

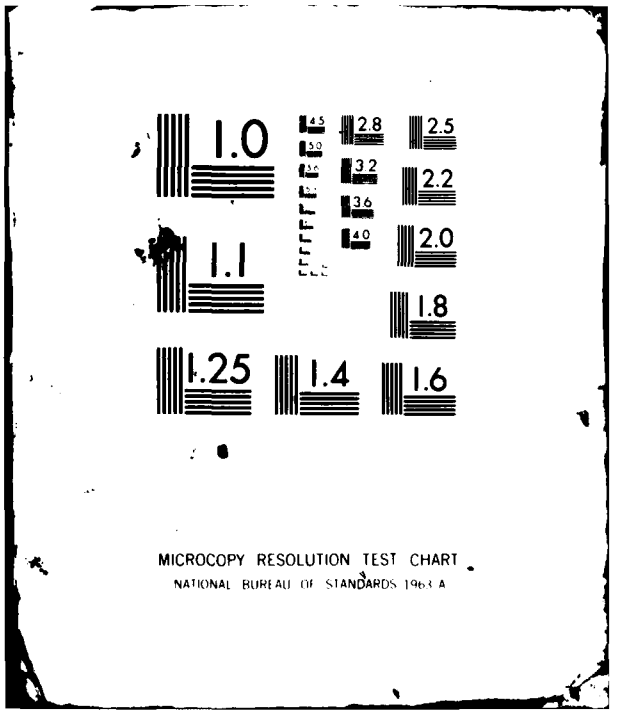
1.0
1.1
1.25
1.4
1.6
1.8
2.0
2.2
2.5
2.8
3.2
3.6
4.0
4.5
5.0
MICROCOPY RESOLUTION TEST CHART
NATIONAL BUREAU OF STANDARDS 1963 A

AD A112089

(6)

A SPLINE SOLUTION OF THE INCOMPRESSIBLE PARABOLIZED NAVIER-STOKES EQUATIONS IN A SHEARED COORDINATE SYSTEM

G. H. Hoffman

Technical Memorandum
File No. TM82-51
25 January 1982
Contract No. N00024-79-C-6043

Copy No. 7

The Pennsylvania State University
APPLIED RESEARCH LABORATORY
Post Office Box 30
Contract No. N00024-79-C-6043

Copy No. _____

Approved for Public Release.
Distribution Unlimited.

DTIC
MAR 18 1982
E

NAVY DEPARTMENT

NAVAL SEA SYSTEMS COMMAND

DTIC FILE COPY

82 3 007

UNCLASSIFIED

SECURITY CLASSIFICATION OF THIS PAGE (When Data Entered)

REPORT DOCUMENTATION PAGE	READ INSTRUCTIONS BEFORE COMPLETING FORM
1. REPORT NUMBER: TM 82-51	2. GOVT ACCESSION NO.: AD-A112 089
3. RECIPIENT'S CATALOG NUMBER	
4. TITLE (and Subtitle): A SPLINE SOLUTION OF THE INCOMPRESSIBLE PARABOLIZED NAVIER-STOKES EQUATIONS IN A SHEARED COORDINATE SYSTEM	5. TYPE OF REPORT & PERIOD COVERED: Technical Memorandum
	6. PERFORMING ORG. REPORT NUMBER
7. AUTHOR(s): G. H. Hoffman	8. CONTRACT OR GRANT NUMBER(s): N00024-79-C-6043
9. PERFORMING ORGANIZATION NAME AND ADDRESS: APPLIED RESEARCH LABORATORY P. O. Box 30 State College, PA 16801	10. PROGRAM ELEMENT, PROJECT, TASK AREA & WORK UNIT NUMBERS
11. CONTROLLING OFFICE NAME AND ADDRESS: Naval Sea Systems Command - Code NSEA-63R31 Department of the Navy Washington, DC 20362	12. REPORT DATE: 25 January 1982 13. NUMBER OF PAGES: 59
14. MONITORING AGENCY NAME & ADDRESS (if different from Controlling Office)	15. SECURITY CLASS. (of this report): UNCLASSIFIED 15a. DECLASSIFICATION/DOWNGRADING SCHEDULE

16. DISTRIBUTION STATEMENT (of this Report)

Approved for Public Release.
Distribution Unlimited.
Per NAVSEA- March 8, 1982.

17. DISTRIBUTION STATEMENT (of the abstract entered in Block 20, if different from Report)

18. SUPPLEMENTARY NOTES

19. KEY WORDS (Continue on reverse side if necessary and identify by block number)

laminar flow, numerical, spline, solution

20. ABSTRACT (Continue on reverse side if necessary and identify by block number)

A model strong interaction problem for two-dimensional laminar flow is solved numerically. The method makes use of the parabolized vorticity approximation in conjunction with fourth-order accurate polynomial splines to resolve the wall shear layer with a relatively sparse grid. A sheared wall fitted coordinate mapping is used which produces discontinuous coefficients in the governing differential equations. These discontinuities

(continuing)

DD FORM 1 JAN 73 1473 EDITION OF 1 NOV 65 IS OBSOLETE

UNCLASSIFIED

SECURITY CLASSIFICATION OF THIS PAGE (When Data Entered)

No. 20 - Continued

are treated in an exact way numerically. The spline-finite difference equations, which result from the discretization, are solved as a coupled system by single line overrelaxation plus a Newton-Raphson iteration to take care of the nonlinearity. Numerical results are presented for six cases consisting of five wall geometries and two Reynolds numbers (10^4 and 10^5). Comparisons are made with potential flow-boundary layer calculations. The method is found to be an efficient way of treating the model strong inter interaction problem even when thin separated zones are present.

DTIC COPY INSPECTED 2

Accession For
NTIS GRA&I [X]
DTIC TAB [ ]
Unannounced [ ]
Justification
By
Distribution/
Availability Codes
Dist | Avail and/or Special
A

Subject: A Spline Solution of the Incompressible Parabolized Navier-Stokes Equations in a Sheared Coordinate System

References: See page 41

Abstract:

A model strong interaction problem for two-dimensional laminar flow is solved numerically. The method makes use of the parabolized vorticity approximation in conjunction with fourth-order accurate polynomial splines to resolve the wall shear layer with a relatively sparse grid. A sheared wall fitted coordinate mapping is used which produces discontinuous coefficients in the governing differential equations. These discontinuities are treated in an exact way numerically. The spline-finite difference equations, which result from the discretization, are solved as a coupled system by single line overrelaxation plus a Newton-Raphson iteration to take care of the nonlinearity. Numerical results are presented for six cases consisting of five wall geometries and two Reynolds numbers (10^4 and 10^5). Comparisons are made with potential flow-boundary layer calculations. The method is found to be an efficient way of treating the model strong interaction problem even when thin separated zones are present.

Acknowledgment: This work was sponsored by the Naval Sea Systems Command, Code NSEA-63R31.

TABLE OF CONTENTS

LIST OF FIGURES

LIST OF TABLES

NOMENCLATURE

c_f wall friction coefficient $= \dfrac{\tau_w^*}{\frac{1}{2}\rho^* U_\infty^{*2}}$

c_{p_w} wall pressure coefficient $= \dfrac{p_w^*}{\frac{1}{2}\rho^* U_\infty^{*2}}$

ℓ^ψ spline derivative approximation of $\dfrac{\partial \psi}{\partial n}$

ℓ^ζ spline derivative approximation of $\dfrac{\partial \zeta}{\partial n}$

L^ψ spline derivative approximation of $\dfrac{\partial^2 \psi}{\partial n^2}$

L^ζ spline derivative approximation of $\dfrac{\partial^2 \zeta}{\partial n^2}$

L^* reference length (dimensional)

n transformed normal coordinate

Δn step size in n-direction

p_w^* wall static pressure (dimensional)

Re Reynolds number $= \dfrac{U_\infty^* L^*}{\nu^*}$

s transformed axial coordinate

Δs step size in s-direction

U_∞^* free-stream speed (dimensional)

x	axial coordinate
x_0	axial coordinate of initial line in computational domain
x_1	axial coordinate of end of region I in computational domain
x_2	axial coordinate of end of region II in computational domain
x_f	axial coordinate of end of computational domain
y	normal coordinate
y_e	normal coordinate of outer edge of computational domain
y_w	normal coordinate of wall
y_w'	first derivative of wall coordinate with respect to x
y_w''	second derivative of wall coordinate with respect to x
y_{w_1}	normal coordinate of front plate
y_{w_2}	normal coordinate of rear plate
u	velocity component in x-direction
v	velocity component in y-direction
δ_0	boundary-layer thickness at $x = x_0$
ψ	stream function
ζ	vorticity magnitude
σ	step size ratio in n direction—see Eq. (42)
η	Blasius similarity variable—see Eq. (100)
τ_w^*	wall shear stress (dimensional)
ν^*	kinematic viscosity (dimensional)
ρ^*	fluid density (dimensional)

All other quantities are defined in the text.

All quantities in the text are made dimensionless as follows:

distance by L^*

velocities by U_∞^*

stream function by $L^* U_\infty^*$

vorticity by U_∞^*/L^*

I. INTRODUCTION

The motivation for the present study is the development of an efficient numerical calculation procedure for flows at moderate to high Reynolds numbers where a strong interaction exists between a boundary layer and a surrounding vorticity-free flow. One possibility for achieving efficiency might be to solve a set of equations which is simpler than the Navier-Stokes equations. In this regard, a number of papers have been published in recent years [5-8]* which show that strong interaction flow fields may be calculated with considerable accuracy by using an approximate set of equations referred to as the parabolized or thin-layer Navier-Stokes equations.

Four parabolic models of the Navier-Stokes equations are possible, according to Davis and Rubin [1]. At the top of this hierarchy, and the one addressed in this report, is the parabolized vorticity equation approximation. In this approximation, the Navier-Stokes equations are written, preferably, in an optimal or nearly optimal coordinate system. Then all terms that make the vorticity equation elliptic are neglected, while all terms in the elliptic stream function equation are retained in order to allow for a proper interaction between the viscid and inviscid layers.

As discussed by Davis [2], the accuracy of a parabolic model depends on the choice of coordinates. Thus, optimal coordinates in the sense of Kaplun [3], provides the best accuracy for the parabolic model, as demonstrated in the calculations of Davis and Rout [4]. The determination of optimal coordinates is itself a formidable task because a complicated set of coupled flow and coordinate equations must be solved. Studies of the parabolized vorticity model using conformal coordinates (which are nearly optimal) have been made by Davis [5], Ghia and Davis [6] and Napolitano, Werle and Davis [7]. These results, even when separated zones are present, are nearly identical to full Navier-Stokes solutions at intermediate and high Reynolds numbers. The work of Steger [8] for high Reynolds number compressible viscous/turbulent flow about an airfoil using the parabolized vorticity approximation indicates that accurate results can even be obtained for numerically generated grids that are slightly non-orthogonal and not chosen from optimality considerations.

The present work provides a further test of the accuracy of the parabolized vorticity approximations in a non-optimal coordinate system as applied to the calculation of strongly interacting flows at intermediate to high Reynolds numbers. Toward this end, the following problem is solved: A steady, incompressible, two-dimensional, laminar flow exists over two flat plates aligned with the oncoming stream, but separated vertically and horizontally. The plates are joined by a smooth center section described by a cubic so that the wall has continuous slopes at the junctures. The pressure distribution in the boundary layer thus may be varied by changing the vertical and horizontal spacing of the fore and aft plates.

---

*Numbers in brackets [] indicate References, see Page 41.

The computational domain for this problem is shown schematically in Fig. 1. On the initial surface at $x = x_o$, measured from the leading edge of the first plate, a Blasius boundary layer exists between $y = 0$ and $y = \delta_o$ (zone 1). Between $y = \delta_o$ and $y = y_e$, the outer edge of the computational domain, a uniform flow is present (zone 2). To ensure that a strong interaction takes place between the boundary layer and the outer inviscid flow, zone 1 is taken to be a significant fraction of zone 2 and the line $y = y_e$ is taken to be a streamline. Actually, the problem posed is the lower half of a diffuser flow that is not fully developed.

The method used here to generate a non-optimal wall-fitted coordinate system is to apply a shearing transformation to the computational domain, shown in Fig. 1, which maps this domain into a rectangle. The vertical distance between the two plates, $y_{w_1} - y_{w_2}$, is restricted to be much less than the horizontal distance, $x_2 - x_1$, to keep separated flow zones thin so as not to violate the parabolic approximation. Consequently, the coordinate system is only mildly non-orthogonal. A typical sheared grid is shown in Fig. 2.

The numerical solution strategy adopted to solve the above problem is along the lines of Murphy [9] in his development of an efficient Navier-Stokes solver. The main features are:

1. The steady parabolized vorticity model is solved using line overrelaxation in conjunction with the Newton-Raphson technique.

2. Fourth-order spline discretization is used in the direction normal to the main flow so that the region of high flow gradients near the wall can be resolved with relatively few grid points. Standard second-order finite difference discretization is then used in the main flow direction where flow gradients are expected to be mild.

The classical Peaceman-Rachford ADI procedure [10], used in References 4-7, requires an orthogonal coordinate system for stability. For non-orthogonal coordinates, a more general splitting technique, such as that of Beam and Warming [11], must be used. On the other hand, SLOR, the procedure used here, is a straightforward and well-proven alternative for obtaining steady solutions which is not affected by mild non-orthogonality of the coordinate system.

Spline collocation techniques as a means of discretizing viscous flow problems have been extensively studied by Rubin and Khosla [12, 13]. They point out the following advantages of the spline formulation over three or five point finite difference discretization:

1. The discretized equations formed with splines remain block tridiagonal.

2. The treatment of derivative boundary conditions is more straightforward because the derivatives are treated as unknowns.

3. A highly nonuniform grid produces less deterioration in accuracy than with finite differences.

4. For equal accuracy the fourth-order spline requires one-fourth the number of grid points in a given direction compared to second-order finite differences.

The disadvantages of splines are that the discretized equations are more complicated than their finite difference counterparts and the storage requirements are larger for a given number of mesh points. Since fewer points are required for comparable accuracy, the spline approach is still the more efficient.

The present discretization is similar to that of Murphy [9], who used a generalized Galerkin technique with splined Taylor series expansions to achieve fourth-order accuracy in the direction normal to the main flow. The use of fourth-order splines achieves essentially the same result but with less algebra to arrive at the numerical algorithm.

This report covers numerical solutions using the parabolized vorticity approximation as well as boundary-layer solutions to show the magnitude of the strong interaction effect. A later report will present comparisions of full Navier-Stokes solutions with the parabolized vorticity model.

II. ANALYSIS

Governing Differential Equations

The starting point of the analysis is the steady, incompressible Navier-Stokes equations written in Cartesian coordinates. In dimensionless stream function-vorticity form these equations are:

Stream Function

$$\psi_{xx} + \psi_{yy} = - \zeta \quad . \tag{1}$$

Vorticity

$$\psi_y \zeta_x - \psi_x \zeta_y = \frac{1}{Re} (\zeta_{xx} + \zeta_{yy}) \quad . \tag{2}$$

where subscripts denote partial differentiation with respect to the subscripted variable. For the truncated computational domain, shown in Fig. 1, the boundary conditions are similar to those of Murphy [9]. At $x = x_0$, the flow is prescribed:

$$\psi = \psi(x_0,y) \quad , \tag{3a}$$

$$\zeta = \zeta(x_0,y) \quad . \tag{3b}$$

At $y = y_w(x)$ the no-slip and impervious wall conditions prevail:

$$u = v = 0 \quad \text{at} \quad y = y_w(x) \quad ,$$

which are equivalent to

$$\psi(x,y_w) = 0 \quad , \tag{4a}$$

$$\psi_y(x,y_w) = 0 \quad . \tag{4b}$$

At $y = y_e$, the outer edge of the domain, the stream function, and vorticity are prescribed:

$$\psi(x,y_e) = \psi_e(x) \quad , \tag{5a}$$

$$\zeta(x,y_e) = \zeta_e(x) \quad , \tag{5b}$$

where usually $\zeta_e = 0$. At the downstream boundary, $x = x_f$, the elliptic region is terminated. Thus

$$\psi_{xx}(x_f,y) = 0 \quad , \tag{6a}$$

$$\zeta_{xx}(x_f,y) = 0 \quad . \tag{6b}$$

These last two conditions are equivalent to requiring the flow to satisfy boundary-layer equations at the outflow boundary.

To produce a wall-fitted coordinate system, the following shearing transformation is used:

$$s = \int [1 + y_w'^2]^{1/2} \, dx \quad , \tag{7}$$

$$n = \phi(x) \cdot y - \lambda(x) \quad , \tag{8}$$

where:

$$\phi(x) = \frac{1}{y_e - y_w(x)} \quad , \tag{9}$$

$$\lambda(x) = \frac{y_w(x)}{y_e - y_w(x)} = \phi\, y_w \quad . \tag{10}$$

and the prime in Eq. (7) denotes differentiation with respect to x. Thus, s corresponds to arc length along the wall and n, the normal variable, ranges between 0 and 1 as y ranges between y_w and y_e. The computational domain is, therefore, mapped into the rectangle $s_0 \leq s \leq s_f$, $0 \leq n \leq 1$.

The transformed Navier-Stokes equations in (s,n) variables are, noting that $s_y = s_{yy} = 0$:

Stream Function

$$s_x^2 \psi_{ss} + 2s_x n_x \psi_{sn} + (n_x^2 + n_y^2)\, \psi_{nn} + s_{xx}\, \psi_s + n_{xx} \psi_n + \zeta = 0 \quad . \tag{11}$$

Vorticity

$$s_x n_y (\psi_n \zeta_s - \psi_s \zeta_n) = \frac{1}{Re} [s_x^2 \zeta_{ss} + 2s_x n_x \zeta_{sn} + (n_x^2 + n_y^2)\, \zeta_{nn} + s_{xx}\, \zeta_s + n_{xx}\, \zeta_n] \quad . \tag{12}$$

The metric coefficients s_x, n_x, etc., obtained from Eqs. (7) and (8), are derived in the Appendix.

The parabolized form of the vorticity equation is obtained from Eq. (12) by dropping ζ_{ss} and ζ_{sn}. To be consistent, the term $s_{xx}\, \zeta_s$ is also dropped. The result is:

Parabolized Vorticity

$$s_x n_y (\psi\, \zeta_s - \psi_s \zeta_n) = \frac{1}{Re} [(n_x^2 + n_y^2)\zeta_{nn} + n_{xx} \zeta_n] \quad . \tag{13}$$

The flow in the computational domain, $s_0 \leq s \leq s_f$, $0 \leq n \leq 1$, is governed by Eqs. (11) and (13).

The boundary conditions in (s,n) coordinates are as follows:

$$\psi = \psi(s_0,n) \quad , \tag{14a}$$

$$\zeta = \zeta(s_0,n) \quad . \tag{14b}$$

on the wall, n = 0:

$$\psi(s,0) = 0 \quad , \tag{15a}$$

$$\psi_n(s,0) = 0 \quad . \tag{15b}$$

On the outer edge, n = 1:

$$\psi(s,1) = \psi_e(s) \quad , \tag{16a}$$

$$\zeta(s,1) = \zeta_e(s) \tag{16b}$$

On the downstream boundary, $s = s_f$, the vorticity equation requires no boundary condition because it is parabolic. The only boundary condition required is

$$\psi_{ss}(s_f, n) = 0 \quad , \tag{17}$$

which applies to the stream function equation.

Spline-Finite Difference Equations in the Field

To use spline approximations in the n-direction, the following spline derivatives must be defined:

$$\ell^{\psi} = \psi_n \quad , \tag{18}$$

$$L^{\psi} = \psi_{nn} \quad , \tag{19}$$

$$\ell^{\zeta} = \zeta_n \quad , \tag{20}$$

$$L^{\zeta} = \zeta_{nn} \quad . \tag{21}$$

The stream function and parabolized vorticity can then be viewed as equations from which to determine L^{ψ} and L^{ζ}. From Eq. (11) one obtains

$$L^{\psi} = - a\, \ell_s^{\psi} - b\, \psi_{ss} - c\, \psi_s - d\, \ell^{\psi} - e\, \zeta \quad , \tag{22}$$

and from Eq. (13),

$$L^{\zeta} = -d\, \ell^{\zeta} + f(\ell^{\psi}\zeta_s - \ell^{\zeta}\psi_s) \quad , \tag{23}$$

where:

$$a = \frac{2\, s_x\, n_x}{n_x^2 + n_y^2} \quad , \tag{24}$$

$$b = \frac{s_x^2}{n_x^2 + n_y^2} \quad , \tag{25}$$

$$c = \frac{s_{xx}}{n_x^2 + n_y^2} \quad , \tag{26}$$

$$d = \frac{n_{xx}}{n_x^2 + n_y^2} \quad , \tag{27}$$

$$e = \frac{1}{n_x^2 + n_y^2} \quad , \tag{28}$$

$$f = \frac{Re\, s_x\, n_y}{n_x^2 + n_y^2} \quad . \tag{29}$$

Note that the cross derivative ψ_{sn} in Eq. (11) has been treated as ℓ_s^{ψ}.

Equations (22) and (23) are now discretized in the s-direction as follows:

1. A constant step size Δs is used for simplicity.

2. In the stream function equation (L^{ψ}), second-order accurate central differences are used.

3. In the parabolized vorticity equation (L^{ζ}), three-point backward differences are used to maintain stability [9].

At line i, the appropriate finite difference expressions for s-derivatives to be used in Eq. (22) are

$$(F_s)_i = \frac{F_{i+1} - F_{i-1}}{2\Delta s} + O(\Delta s^2) \quad , \tag{30}$$

$$(F_{ss})_i = \frac{F_{i-1} - 2F_i + F_{i+1}}{\Delta s^2} + O(\Delta s^2) \quad , \tag{31}$$

and in Eq. (23),

$$(F_s)_i = \frac{F_{i-2} - 4F_{i-1} + 3F_i}{2\Delta s} + O(\Delta s^2) \quad . \tag{32}$$

Considering quantities at node point (i,j), corresponding to (s_i, n_j), as unknowns, Eqs. (22) and (23), with the aid of Eqs. (30)-(32), can be written as

$$L^{\psi}_{i,j} = \frac{2b_{i,j}}{\Delta s^2}\psi_{i,j} - d_{i,j}\,\ell^{\psi}_{i,j} - e_{i,j}\,\zeta_{i,j} + P_{i,j} \quad , \tag{33}$$

where

$$P_{i,j} = -\frac{1}{\Delta s^2}\left[\left(b_{i,j} - \frac{c_{i,j}\Delta s}{2}\right)\psi_{i-1,j} + \left(b_{i,j} + \frac{c_{i,j}\Delta s}{2}\right)\psi_{i+1,j}\right]$$

$$- \frac{a_{i,j}}{2\Delta s}\left(\ell^{\psi}_{i+1,j} - \ell^{\psi}_{i-1,j}\right) \quad , \tag{34}$$

and

$$L^{\zeta}_{i,j} = -\hat{A}_{i,j}\cdot\ell^{\zeta}_{i,j} + \hat{B}_{i,j}\cdot\ell^{\psi}_{i,j}$$

$$+ \frac{3f_{i,j}}{2\Delta s}\left(\ell^{\psi}\zeta - \ell^{\zeta}\psi\right)_{i,j} \quad , \tag{35}$$

where

$$\hat{A}_{i,j} = d_{i,j} + \frac{f_{i,j}}{2\Delta s} (\psi_{i-2,j} - 4\psi_{i-1,j}) \tag{36}$$

$$\hat{B}_{i,j} = \frac{f_{i,j}}{2\Delta s} (\zeta_{i-2,j} - 4\zeta_{i-1,j}) \quad . \tag{37}$$

The number of unknowns at (i,j) is six, namely: ψ, ℓ^{ψ}, L^{ψ}, ζ, ℓ^{ζ} and L^{ζ}. Therefore, Eqs. (33) and (35) must be supplemented by four spline relations to close the system. To produce a compact fourth-order accurate system, $S^1(4,0)$ is used four times: (1) to relate ψ to ℓ^{ψ}, (2) to relate ℓ^{ψ} to L^{ψ}, (3) to relate ζ to ℓ^{ζ}, and (4) to relate ℓ^{ζ} to L^{ζ}. The $S^1(4,0)$ tridiagonal relationship may be written [12]

$$AA_j \, F_{i,j-1} + \sigma^2 \, \ell^F_{i,j-1} + BB_j \, F_{i,j} + (1+\sigma)^2 \, \ell^F_{i,j}$$

$$+ CC_j \, F_{i,j+1} + \ell^F_{i,j+1} = 0 \quad , \tag{38}$$

where F denotes ψ or ℓ^{ψ} or ζ or ℓ^{ζ}, and

$$AA_j = \frac{2\sigma^2(2+\sigma)}{\Delta n_{j-1}(1+\sigma)} \quad , \tag{39}$$

$$BB_j = \frac{2(1-\sigma)(1+\sigma)^2}{\Delta n_{j-1}\sigma} \quad , \tag{40}$$

$$CC_j = -\frac{2(1+2\sigma)}{\Delta n_{j-1}(1+\sigma)\sigma} \quad , \tag{41}$$

$$\sigma = \sigma_j = \frac{\Delta n_j}{\Delta n_{j-1}} \quad , \tag{42}$$

$$\Delta n_j = n_{j+i} - n_j \tag{43}$$

The number of unknowns at node (i,j) can be reduced from six to four by substitution of the expression for $L^{\psi}_{i,j}$, Eq. (33), and $L^{\zeta}_{i,j}$, Eq. (35), into the splines relating ℓ^{ψ} to L^{ψ} and ℓ^{ζ} to L^{ζ}. A nonlinear block tridiagonal system results which is then linearized for solution by the Newton-Raphson technique. If superscript n denotes the interior iteration number, associated with the nonlinear spline-finite difference (SFD) equations on line i, and F denotes one of the four unknowns ψ, ℓ^{ψ}, ζ, ℓ^{ζ}, then

$$F^{(n+1)} = F^{(n)} + \delta F^{(n)} \quad , \tag{44}$$

where $\delta F^{(n)}$ is assumed to be a small correction. The linearized system is obtained by substituting Eq. (44) into the nonlinear system, neglecting squares of $\delta F^{(n)}$ and writing the result in terms of the corrections. By solving for the corrections rather than the functional values themselves, the cancellation errors are reduced [14]. The linearized set of SFD equations is as follows: (the n superscript is understood.)

$$
\begin{aligned}
&-\left(\frac{3f_{i,j-1}\sigma^2}{2\Delta s}\,\ell^{\zeta}_{i,j-1}\right)\delta\psi_{i,j-1}+\left[\sigma^2\left(B_{i,j-1}+\frac{3f_{i,j-1}}{2\Delta s}\,\zeta_{i,j-1}\right)\right]\delta\ell^{\psi}{}_{i,j-1}\\
&+\left(\frac{3f_{i,j-1}\sigma^2}{2\Delta s}\,\ell^{\psi}_{i,j-1}\right)\delta\zeta_{i,j-1}+\left[AA_j-\sigma^2\left(\hat{A}_{i,j-1}+\frac{3f_{i,j-1}}{2\Delta s}\,\psi_{i,j-1}\right)\right]\delta\ell^{\zeta}{}_{i,j}\\
&-\left[\frac{3f_{i,j}(1+\sigma)^2}{2\Delta s}\,\ell^{\zeta}_{i,j}\right]\delta\psi_{i,j}+\left[(1+\sigma)^2\left(\hat{B}_{i,j}+\frac{3f_{i,j}}{2\Delta s}\,\zeta_{i,j}\right)\right]\delta\ell^{\psi}{}_{i,j}\\
&+\left[\frac{3f_{i,j}(1+\sigma)^2}{2\Delta s}\,\ell^{\psi}_{i,j}\right]\delta\zeta_{i,j}+\left[BBj-(1+\sigma)^2\left(\hat{A}_{i,j}+\frac{3f_{i,j}}{2\Delta s}\,\psi_{i,j}\right)\right]\delta\ell^{\zeta}{}_{i,j}\\
&-\left(\frac{3f_{i,j+1}}{2\Delta s}\,\ell^{\zeta}_{i,j+1}\right)\delta\psi_{i,j+1}+\left[\hat{B}_{i,j+1}+\frac{3f_{i,j+1}}{2\Delta s}\,\zeta_{i,j+1}\right]\delta\ell^{\psi}_{i,j+1}\\
&+\left(\frac{3f_{i,j+1}}{2\Delta s}\,\ell^{\psi}_{i,j+1}\right)\delta\zeta_{i,j+1}+\left[CC_j-\hat{A}_{i,j+1}-\frac{3f_{i,j+1}}{2\Delta s}\,\psi_{i,j+1}\right]\delta\ell^{\zeta}{}_{i,j+1}\\
&=Dl_{i,j} \quad ,
\end{aligned}
\tag{45}
$$

and

$$\left(\frac{2b_{i,j-1}\sigma^2}{\Delta s^2}\right) \delta\psi_{i,j-1} + (AA_j - \sigma^2 d_{i,j-1})\, \delta\ell^{\psi}_{i,j-1} - (\sigma^2 e_{i,j-1})\, \delta\zeta_{i,j-1}$$

$$+ \left[\frac{2b_{i,j}(1+\sigma)^2}{\Delta s^2}\right] \delta\psi_{i,j} + \left[BB_j - (1+\sigma)^2 d_{i,j}\right] \delta\ell^{\psi}_{i,j} - \left[(1+\sigma)^2 e_{i,j}\right] \delta\zeta_{i,j}$$

$$+ \left(\frac{2b_{i,j+1}}{\Delta s^2}\right) \delta\psi_{i,j+1} + (CC_j - d_{i,j+1})\, \delta\ell^{\psi}_{i,j+1} - (e_{i,j+1})\, \delta\zeta_{i,j+1}$$

$$= D2_{i,j} \quad , \tag{46}$$

and

$$AA_j\, \delta\psi_{i,j-1} + \sigma^2 \ell^{\psi}_{i,j-1} + BB_j\, \delta\psi_{i,j} + (1+\sigma)^2\, \delta\ell^{\psi}_{i,j}$$

$$+ CC_j\, \delta\psi_{i,j+1} + \delta\ell^{\psi}_{i,j+1} = D3_{i,j} \tag{47}$$

and

$$AA_j\, \delta\zeta_{i,j-1} + \sigma^2 \delta\ell^{\zeta}_{i,j-1} + BB_j\, \delta\zeta_{i,j} + (1+\sigma)^2\, \delta\ell^{\zeta}_{i,j}$$

$$+ CC_j\, \delta\zeta_{i,j+1} + \delta\ell^{\zeta}_{i,j+1} = D4_{i,j} \quad . \tag{48}$$

The right-hand sides of Eqs. (45)-(48) are given by

$$D1_{i,j} = -\sigma^2 \hat{B}_{i,j-1}\, \ell^{\psi}_{i,j-1} - (AA_j - \sigma^2 \hat{A}_{i,j-1})\, \ell^{\zeta}_{i,j-1}$$

$$- \frac{3f_{i,j-1}\sigma^2}{2\Delta s} (\ell^{\psi}\zeta - \ell^{\zeta}\psi)_{i,j-1} - (1+\sigma)^2\, \hat{B}_{i,j}\, \ell^{\psi}_{i,j} - [BB_j - (1+\sigma)^2 \hat{A}_{i,j}]\, \ell^{\zeta}_{i,j}$$

$$- \frac{3f_{i,j}(1+\sigma)^2}{2\Delta s} (\ell^{\psi}\zeta - \ell^{\zeta}\psi)_{i,j} - \hat{B}_{i,j+1} \ell^{\psi}_{i,j+1} - (CC_j - \hat{A}_{i,j+1})\, \ell^{\zeta}_{i,j+1}$$

$$- \frac{3f_{i,j+1}}{2\Delta s} (\ell^{\psi}\zeta - \ell^{\zeta}\psi)_{i,j+1} \quad , \tag{49}$$

and

$$D2_{i,j} = -\sigma^2 P_{i,j-1} - (1+\sigma)^2 P_{i,j} - P_{i,j+1} - \frac{2b_{i,j-1}\sigma^2}{\Delta s^2}\psi_{i,j-1}$$

$$- (AA_j - \sigma^2 d_{i,j-1})\,\ell^{\psi}_{i,j-1} + \sigma^2 e_{i,j-1}\,\zeta_{i,j-1} - \frac{2b_{i,j}(1+\sigma)^2}{\Delta s^2}\psi_{i,j}$$

$$- [BB_j - (1+\sigma)^2 d_{i,j}]\,\ell^{\psi}_{i,j} + (1+\sigma)^2 e_{i,j}\,\zeta_{i,j} - \frac{2b_{i,j+1}}{\Delta s^2}\psi_{i,j+1}$$

$$- (CC_j - d_{i,j+1})\,\ell^{\psi}_{i,j+1} + e_{i,j+1}\,\zeta_{i,j+1} \quad , \tag{50}$$

and

$$D3_{i,j} = -AA_j\psi_{i,j-1} - \sigma^2\ell^{\psi}_{i,j-1} - BB_j\,\psi_{i,j} - (1+\sigma)^2\,\ell^{\psi}_{i,j}$$

$$- CC_j\psi_{i,j+1} - \ell^{\psi}_{i,j+1} \quad , \tag{51}$$

and

$$D4_{i,j} = -AA_j\,\zeta_{i,j-1} - \sigma^2\ell^{\zeta}_{i,j-1} - BB_j\,\zeta_{i,j} - (1+\sigma)^2\,\ell^{\zeta}_{i,j}$$

$$- CC_j\,\zeta_{i,j+1} - \ell^{\zeta}_{i,j+1} \quad . \tag{52}$$

The linearized block tridiagonal system for the corrections may be written as the following matrix equation along line i.

$$-A_j\,z_{j-1} + B_j\,z_j - C_j\,z_{j+1} = D_j \quad , \quad 2 \le j \le N \quad , \tag{53}$$

where N is the number of intervals in the n direction, z_j is the four component correction vector defined by

$$z^T_{i,j} = [\delta\psi,\ \delta\ell^{\psi},\ \delta\zeta,\ \delta\ell^{\zeta}]_{i,j} \quad , \tag{54}$$

and A, B, and C are 4x4 matrices whose elements are obtained from Eqs. (45)-(48). Finally, D_j is a four-component column vector of known quantities with components $(D1, D2, D3, D4)_{i,j}$ given by Eqs. (49)-(52).

Spline-Finite Difference Equations at the Wall

The boundary conditions on the wall, Eqs. (15a) and (15b), in SFD form are

$$\psi_{i,1} = 0 \quad , \tag{55}$$

$$\ell^{\psi}_{i,1} = 0 \quad . \tag{56}$$

Two spline relations are needed to close the system. These are obtained from Eq. (15) of Rubin and Khosla [12]. This spline relation, obtained from differentiation of $S^1(4,0)$, is a two-point formula with fourth-order truncation error. Applied to the present case one has the following two equations:

$$\frac{6}{\Delta n_1^2}(\psi_{i,2} - \psi_{i,1}) - \frac{2}{\Delta n_1}(2\ell^{\psi}_{i,1} + \ell^{\psi}_{i,2}) - L^{\psi}_{i,1} = 0 \quad , \tag{57}$$

and

$$\frac{6}{\Delta n_1^2}(\zeta_{i,2} - \zeta_{i,1}) - \frac{2}{\Delta n_1}(2\ell^{\zeta}_{i,1} + \ell^{\zeta}_{i,2}) - L^{\zeta}_{i,1} = 0 \quad . \tag{58}$$

The spline second derivatives $L^{\psi}_{i,1}$ and $L^{\zeta}_{i,1}$ are eliminated by using Eqs. (33) and (35) evaluated at $j = 1$.

Substitution of Eq. (35) into Eq. (58) gives a nonlinear equation which is linearized as described previously. The system of four linear equations at the wall written in terms of corrections is as follows:

$$\delta\psi_{i,1} = D1_{i,1} \quad , \tag{59}$$

and

$$\delta\ell^{\psi}_{i,1} = D2_{i,1} \quad , \tag{60}$$

and

$$-\left(\frac{6}{\Delta n_1^2} + \frac{2b_{i,1}}{\Delta s^2}\right)\delta\psi_{i,1} - \left(\frac{4}{\Delta n_1} - d_{i,1}\right)\delta\ell^{\psi}_{i,1} + e_{i,1}\,\delta\zeta_{i,1} + \frac{6}{\Delta n_1^2}\delta\psi_{i,2}$$

$$-\frac{2}{\Delta n_1}\delta\ell^{\psi}_{i,2} = D3_{i,1} \quad , \tag{61}$$

and

$$\left(\frac{3f_{i,1}}{2\Delta s}\,\ell^{\zeta}_{i,1}\right)\delta\psi_{i,1} - \left(\hat{B}_{i,1} + \frac{3f_{i,1}}{2\Delta s}\,\zeta_{i,1}\right)\delta\ell^{\psi}_{i,1} - \left(\frac{6}{\Delta n_1^{\,2}} + \frac{3f_{i,1}}{2\Delta s}\,\ell^{\psi}_{i,1}\right)\delta\zeta_{i,1}$$

$$+ \left(\hat{A}_{i,1} + \frac{3f_{i,1}}{2\Delta s}\,\psi_{i,1} - \frac{4}{\Delta n_1}\right)\delta\ell^{\zeta}_{i,1} + \frac{6}{\Delta n_1^{\,2}}\,\delta\zeta_{i,2} - \frac{2}{\Delta n_1}\,\delta\ell^{\zeta}_{i,2} = D4_{i,1} \quad . \tag{62}$$

The right-hand sides of Eqs. (59) and (62) are

$$D1_{i,1} = 0 \quad , \tag{63}$$

$$D2_{i,1} = 0 \quad , \tag{64}$$

$$D3_{i,1} = P_{i,1} + \left(\frac{6}{\Delta n_1^{\,2}} + \frac{2b_{i,1}}{\Delta s^2}\right)\psi_{i,1} + \left(\frac{4}{\Delta n_1} - d_{i,1}\right)\ell^{\psi}_{i,1} - e_{i,1}\,\zeta_{i,1}$$

$$- \frac{6}{\Delta n_1^{\,2}}\,\psi_{i,2} + \frac{2}{\Delta n_1}\,\ell^{\psi}_{i,2} \quad , \tag{65}$$

$$D4_{i,1} = \hat{B}_{i,1}\,\ell^{\psi}_{i,1} + \frac{6}{\Delta n_1^{\,2}}\,\zeta_{i,1} + \left(\frac{4}{\Delta n_1} - \hat{A}_{i,1}\right)\ell^{\zeta}_{i,1}$$

$$+ \frac{3f_{i,1}}{2\Delta s}\,(\ell^{\psi}\zeta - \ell^{\zeta}\psi)_{i,1} - \frac{6}{\Delta n_1^{\,2}}\,\zeta_{i,2} + \frac{2}{\Delta n_1}\,\ell^{\zeta}_{i,2} \quad . \tag{66}$$

The quantities $D1_{i,1}$ and $D2_{i,1}$ are both zero provided the correct boundary conditions, Eqs. (55) and (56), are imposed on the first iterate (n = 1).

The linear system, Eqs. (59)-(62), may be written as the following matrix equation.

$$B_1\,z_1 - C_1\,z_2 = D_1 \quad , \tag{67}$$

where, as in the general case, B_1 and C_1 are 4x4 matrices with known elements obtained from Eqs. (59)-(62) and D_1 is a four-component column vector with components given by Eqs. (63)-(66).

Spline-Finite Difference Equations at the Outer Edge

The boundary conditions on the outer edge of the computational domain, Eqs. (16a) and (16b), in SFD form are:

$$\psi_{i,N+1} = \psi_{e_i} \quad , \tag{68}$$

$$\zeta_{i,N+1} = \zeta_{e_i} \quad . \tag{69}$$

Two spline relations are also needed here to close the system. Equation (14) of Rubin and Khosla is the appropriate relation, analogous to the spline used at the wall. Thus,

$$\frac{6}{\Delta n_N^2}\left(\psi_{i,N+1} - \psi_{i,N}\right) - \frac{2}{\Delta n_N}\left(\ell^{\psi}_{i,N} + 2\ell^{\psi}_{i,\,N+1}\right) + L^{\psi}_{i,N+1} = 0 \quad , \tag{70}$$

and

$$\frac{6}{\Delta n_N^2}\left(\zeta_{i,\,N+1} - \zeta_{i,N}\right) - \frac{2}{\Delta n_N}\left(\ell^{\zeta}_{i,N} + 2\ell^{\zeta}_{i,N+1}\right) + L^{\zeta}_{i,N+1} = 0 \quad . \tag{71}$$

Following the procedure used at the wall, $L^{\psi}_{i,\,N+1}$ and $L^{\zeta}_{i,N+1}$ are eliminated by using Eqs. (33) and (35). Then, Eq. (71) is linearized and all four equations, Eqs. (68)-(71), put into the following correction form:

$$\delta\psi_{i,N+1} = D1_{i,N+1} \quad , \tag{72}$$

and

$$\delta\zeta_{i,N+1} = D2_{i,N+1} \quad , \tag{73}$$

and

$$-\frac{6}{\Delta n_N^2}\delta\psi_{i,N} - \frac{2}{\Delta n_N}\delta\ell^{\psi}_{i,N} + \left(\frac{6}{\Delta n_N^2} + \frac{2b_{i,N+1}}{\Delta s^2}\right)\delta\psi_{i,N+1}$$

$$-\left(\frac{4}{\Delta n_N} + d_{i,N+1}\right)\delta\ell^{\psi}_{i,N+1} - e_{i,N+1}\,\delta\zeta_{i,N+1} = D3_{i,N+1} \quad , \tag{74}$$

and

$$-\frac{6}{\Delta n_N^2}\,\delta\zeta_{i,N}-\frac{2}{\Delta n_N}\,\delta\ell^{\zeta}_{i,N}-\left(\frac{3f_{i,N+1}}{2\Delta s}\,\ell^{\zeta}_{i,N+1}\right)\delta\psi_{i,N+1}$$

$$+\left(\hat{B}_{i,N+1}+\frac{3f_{i,N+1}}{2\Delta s}\,\zeta_{i,N+1}\right)\delta\ell^{\psi}_{i,N+1}+\left(\frac{6}{\Delta n_N^2}+\frac{3f_{i,N+1}}{2\Delta s}\,\ell^{\psi}_{i,N+1}\right)\delta\zeta_{i,N+1}$$

$$-\left(\frac{4}{\Delta n_N}+\hat{A}_{i,N+1}+\frac{3f_{i,N+1}}{2\Delta s}\,\psi_{i,N+1}\right)\delta\ell^{\zeta}_{i,N+1}=D4_{i,N+1}\quad . \tag{75}$$

The right-hand sides of Eqs. (72)-(75) are:

$$D1_{i,N+1}=0\quad , \tag{76}$$

$$D2_{i,N+1}=0\quad , \tag{77}$$

$$D3_{i,N+1}=-P_{i,N+1}+\frac{6}{\Delta n_N^2}\,\psi_{i,N}+\frac{2}{\Delta n_N}\,\ell^{\psi}_{i,N}-\left(\frac{6}{\Delta n_N^2}+\frac{2b_{i,N+1}}{\Delta s^2}\right)\psi_{i,N+1}$$

$$+\left(\frac{4}{\Delta n_N}+d_{i,N+1}\right)\ell^{\psi}_{i,N+1}+e_{i,N+1}\,\zeta_{i,N+1}\quad , \tag{78}$$

$$D4_{i,N+1}=\frac{6}{\Delta n_N^2}\,\zeta_{i,N}+\frac{2}{\Delta n_N}\,\ell^{\zeta}_{i,N}-\hat{B}_{i,N+1}\,\ell^{\psi}_{i,N+1}-\frac{6}{\Delta n_N^2}\,\zeta_{i,\,N+1}$$

$$+\left(\frac{4}{\Delta n_N}+\hat{A}_{i,N+1}\right)\ell^{\zeta}_{i,N+1}+\frac{3f_{i,N+1}}{2\Delta s}\,(\ell^{\zeta}\psi-\ell^{\psi}\zeta)_{i,N+1}\quad . \tag{79}$$

In Eqs. (76) and (77) the boundary conditions, Eqs. (68) and (69), are satisfied by the first iterate.

Then, the matrix form of Eqs. (72)-(75) is

$$- A_{N+1} z_N + B_{N+1} z_{n+1} = D_{N+1} \tag{80}$$

where, as before, A_{N+1} and B_{N+1} are 4x4 matrices with known elements, from Eqs. (72)-(75), and D_{N+1} is a four-component column vector of known quantities given by Eqs. (76)-(79).

Solution of Matrix Equations

Equations (53), (67), and (80) form a block tridiagonal system which may be solved by standard lower-upper (L-U) factorization methods, as described by Keller [14]. To avoid buildup of numerical errors when solving the subsidiary 4x4 block systems, pivoting must be used. Blottner [15] has developed a block tridiagonal solver which performs pivoting within the blocks and also minimizes storage requirements associated with the L-U decomposition procedure. The explanation and computer code for this solver appears on pp. 27-32 of Reference 15. Blottner's algorithm has been adapted to the solution of the present system.

Spline-Finite Defference Equations at a Map Junction

The use of sheared coordinates, Eqs. (7) and (8), introduces discontinuities into the metric coefficients along an s = constant line whenever $y_w'(x)$ and/or $y_w''(x)$ are discontinuous. In the present case, only $y_w''(x)$ is discontinuous and, hence, the net effect on the SFD equations is weak. The only equation affected is the stream function equation because central differences are used to approximate the s-derivatives which at a map junction straddle the discontinuity. Consequently, the SFD approximation of the stream function equation takes on a special form at map discontinuities. The parabolized vorticity equation is not affected because it contains only first derivatives in s which are approximated by backward differences that do not straddle the discontinuity.

The map junction will be treated in a general manner by denoting upstream and downstream regions bordering the junction by superscript (k) and (k+1), respectively. At the junction smoothness of the solution requires that ψ and its various derivatives with respect to x and y be continuous. Note that conditions on ζ are not needed. The required smoothness conditions are:

$$\psi_i^{(k)} = \psi_i^{(k+1)} = \psi_i \quad , \tag{81}$$

$$(\psi_y)_i^{(k)} = (\psi_y)_i^{(k+1)} \quad , \tag{82}$$

$$(\psi_{yy})_i^{(k)} = (\psi_{yy})_i^{(k+1)} \quad , \tag{83}$$

$$(\psi_x)_i^{(k)} = (\psi_x)_i^{(k+1)} \quad . \tag{84}$$

Using the chain rule, Eqs. (81)-(84) become

$$(n_y)_i^{(k)} \; (\psi_n)_i^{(k)} = (n_y)_i^{(k+1)} \; (\psi_y)_i^{(k+1)} \quad , \tag{85}$$

$$[(n_y)_i^2]^{(k)} \; (\psi_{nn})_i^{(k)} = [(n_y)_i^2]^{(k+1)} \; (\psi_{nn})_i^{(k+1)} \quad , \tag{86}$$

$$(s_x \psi_s + n_x \psi_n)_i^{(k)} = (s_x \psi_s + n_x \psi_n)_i^{(k+1)} \tag{87}$$

From the Appendix, the metric coefficients in Eqs. (85-(87) are

$$s_x = (1 + y_w'^2)^{1/2} \quad ,$$

$$n_x = y_w' \; (y_e - y_w)^{-1} \; (n - 1) \quad ,$$

$$n_y = (y_e - y_w)^{-1} \quad .$$

At the map junction, $y_{w_i}^{(k)} = y_{w_i}^{(k+1)}$ and $y_{w_i}'^{,(k)} = y_{w_i}'^{,(k+1)} = 0$. Hence, the above metric cooefficients reduce to

$$s_{x_i}^{(k)} = s_{x_i}^{(k+1)} = 1 \quad ,$$

$$n_{x_{i,j}}^{(k)} = n_{x_{i,j}}^{(k+1)} = 0 \quad ,$$

$$n_{yi}^{(k)} = n_{yi}^{(k+1)} = n_{yi} = (y_e - y_{w_i})^{-1} \quad .$$

As a result, smoothness relations Eqs. (85)-(87) simplify to

$$(\psi_n)_i^{(k)} = (\psi_n)_i^{(k+1)} = (\psi_n)_i \quad , \tag{88}$$

$$(\psi_{nn})_i^{(k)} = (\psi_{nn})_i^{(k+1)} = (\psi_{nn})_i \quad , \tag{89}$$

$$(\psi_s)_i^{(k)} = (\psi_s)_i^{(k)} = (\psi_s)_i \quad . \tag{90}$$

In terms of spline variables, Eqs. (88) and (89) may be written

$$\ell_i^{\psi(k)} = \ell_i^{\psi(k+1)} = \ell_i^{\psi} \quad , \tag{91}$$

$$L_i^{\psi(k)} = L_i^{\psi(k+1)} = L_i^{\psi} \quad . \tag{92}$$

To write Eq. (90) in discretized form, region (k) is extended one step into region (k+1) and vice versa resulting in fictitious node lines. Unknowns on these fictitious node lines are denoted by an asterisk (*) superscript. Using CD approximations for ψ_s in Eq. (90), multiplying by $2\Delta s$ and rearranging gives the following result:

$$\psi_{i-1,j}^{*(k+1)} + \psi_{i+1,j}^{*(k)} = \psi_{i-1,j} + \psi_{i+1,j} \quad , \tag{93}$$

where the k superscripts have been omitted from values of ψ lying within their respective regions.

The values of ψ on the fictitious node lines appearing on the left-hand side of Eq. (93) can be eliminated by using the stream function equation evaluated at (i,j), the node point common to both regions (k) and (k+1). Since $y_w' = 0$ at the map junction, the stream function equation simplifies to

$$L^{\psi} + b\,\psi_{ss} + d\,\ell^{\psi} + e\,\zeta = 0 \quad . \tag{94}$$

Upon using a CD approximation for ψ_{ss}, Eq. (94) becomes

$$L_{i,j}^{\psi} + \frac{b_{i,j}}{\Delta s^2}\psi_{i-1,j} - \frac{2b_{i,j}}{\Delta s^2}\psi_{i,j} + \frac{b_{i,j}}{\Delta s^2}\psi_{i+1,j}$$

$$+ d_{i,j}\,\ell_{i,j}^{\psi} + e_{i,j}\,\zeta_{i,j} = 0 \quad . \tag{95}$$

Let the i index at the junction be denoted by IJ and write Eq. (95) at IJ in region (k) to yield

$$\psi_{IJ+1,j}^{*(k)}$$

and at IJ in region (k+1) to yield

$$\psi_{IJ-1,j}^{*(k+1)} \quad .$$

Substitution of these results into Eq. (93) gives the following special form for L^{ψ} on the junction line:

$$L^{\psi}_{IJ,j} = \frac{2b_{IJ,J}}{\Delta s^2}\ \psi_{IJ,j} - \bar{d}_{IJ,j}\ \ell^{\psi}_{i,j} - e_{IJ,j} + P_{IJ,j} \quad , \tag{96}$$

where

$$\bar{d}_{IJ,j} = \frac{1}{2}\left[d^{(k)}_{IJ,j} + d^{(k+1)}_{IJ,j}\right] \quad , \tag{97}$$

$$P_{IJ,j} = -\frac{b_{IJ,j}}{\Delta s^2}\ (\psi_{IJ-1,j} + \psi_{IJ+1,j}) \quad . \tag{98}$$

Equation (96) is seen to be the same as the general case, Eq. (33), provided d is replaced by $\bar{d}$ and P is simplified as above. The quantity $\bar{d}$ (related to n_{xx} and hence y_w'') is the average of d across the junction line. If y_w' had been discontinuous, the same procedure for determining the special expression for L^{ψ} at the junction would have been applicable but a more complicated expression would have resulted. The foregoing treatment of junction lines is a generalization of the method developed by Chmielewski and Hoffman [16].

At the first s = constant line downstream of a map junction, the second-order backward difference used for s-derivatives in the vorticity equation requires knowing the vorticity on the fictitious node line upstream of the junction. To avoid the problematical calculation of this value of vorticity, a first-order backward difference is used. Once this s-line is passed, the scheme reverts to using second-order backward differences.

Starting Solution

As shown in the schematic in Fig. 1, the boundary conditions on the initial line, $s = s_0$, (the starting line) are divided into two zones:

1. Blasius solution, $0 \le y \le \delta_0$.
2. Uniform flow, $\delta_0 \le y \le y_e$.

The Blasius solution, which is assumed to hold between the leading edge ($x = 0$) and the initial line ($x = x_0$), is thus used to obtain the values of ψ, ℓ^{ψ}, ζ and ℓ^{ζ} on $x = x_0$ for $0 \le y \le \delta_0$. The Blasius similarity variables f and η are related to physical variables by

$$\psi = \left(\frac{2x}{Re}\right)^{1/2} f(\eta) \quad , \tag{99}$$

where

$$\eta = \left(\frac{Re}{2x}\right)^{1/2} y \quad . \tag{100}$$

The other three required quantities are:

$$\ell^{\psi} = \frac{f'}{\phi} \quad , \tag{101}$$

$$\zeta = \left(\frac{Re}{2x}\right)^{1/2} f'' \quad , \tag{102}$$

$$\ell^{\zeta} = \frac{Re}{2x} ff'' \quad , \tag{103}$$

where the prime denotes differentiation with respect to η.

The Blasius solution is calculated as follows: The similarity form of the semi-infinite flat plate boundary-layer equation is

$$f''' + ff'' = 0 \quad , \tag{104}$$

with boundary conditions,

$$f = f' = 0 \quad \text{on} \quad \eta = 0 \quad , \tag{105}$$

$$f' = 1 \quad \text{on} \quad \eta = \eta_{\infty} \quad . \tag{106}$$

The differential equation may be written as the following pair of differential equations:

$$u = f' \quad , \tag{107}$$

$$u'' + fu' = 0 \quad . \tag{108}$$

Then, upon introduction of the spline variables:

$$\left.\begin{aligned} \bar{\ell} &= f' \\ \ell &= u' \\ L &= u'' \end{aligned}\right\} \tag{109}$$

the pair of differential equations becomes, at point j:

$$\overline{\ell}_j = u_j \quad , \tag{110}$$

$$L_j = - f_j \ell_j \quad . \tag{111}$$

Since there are five unknowns at j (f, $\overline{\ell}$, u, ℓ and L) three spline relations are needed to close the system. To be consistent with the parabolized solution, $S^1(4,0)$ is used three times and the number of unknowns is reduced to f, u and ℓ by use of Eqs. (110) and (111).

In the uniform flow region outside the boundary layer, the initial flow variables are

$$\psi = \psi_{\delta_0} + y - \delta_0 \quad , \tag{112}$$

$$\ell^\psi = 1 \quad , \tag{113}$$

$$\zeta = 0 \quad , \tag{114}$$

$$\ell^\zeta = 0 \quad , \tag{115}$$

where ψ_{δ_0} is the value of the stream function at $y = \delta_0$, the edge of the Blasius boundary layer.

To eliminate the requirement of two initial lines to start the solution, as required by the three-point backward difference used for s-derivatives in the vorticity equation, a two-point backward difference is used at the first s = constant line downstream of $s = s_0$. Thus, the solution at this line is only first-order accurate in Δs.

Stream Function Equation at the Downstream Boundary

In region II the coefficients a, c and d, given by Eqs. (24), (26) and (27), are zero because $y_w' = y_w'' = 0$. Hence, the spline form of the stream function equation , Eq. 22), reduces to

$$L^\psi = - b\psi_{ss} - e\,\zeta \quad . \tag{116}$$

The downstream boundary condition on ψ that terminates the elliptic region was $\psi_{ss} = 0$ on $s = s_f$. Hence, the SFD form of Eq. (116) on this boundary (i = IMAX) is

$$L^\psi_{IMAX,j} = - e_{IMAX}\,\zeta_{IMAX,j} \quad , \tag{117}$$

which replaces Eq. (33). The matrix coefficients associated with the block tridiagonal system for z on i = IMAX therefore considerably simplify and

$$b_{IMAX,j} = d_{IMAX,j} = P_{IMAX,j} = 0 \quad ,$$

in the appropriate formulas.

Wall Pressure Coefficient

A simple method to obtain the pressure coefficient on the wall is to integrate the s-momentum equation along the wall starting from $s = s_0$ where c_p is assumed to be zero. The derivation begins with the x and y momentum equation evaluated at $y = y_w(x)$, where $u = v = 0$. These equations reduce to

$$\left(\frac{\partial c_p}{\partial x}\right)_w = -\frac{2}{Re}\,(\zeta_y)_w \quad , \tag{118}$$

and

$$\left(\frac{\partial c_p}{\partial y}\right)_w = \frac{2}{Re}\,(\zeta_x)_w \quad , \tag{119}$$

Upon transformation to (s,n) coordinates, these equations become

$$s_x\left(\frac{\partial c_p}{\partial s}\right)_w + n_x\left(\frac{\partial c_p}{\partial n}\right)_w = -\frac{2}{Re}\,\phi\,(\zeta_n)_w \quad , \tag{120}$$

and

$$\phi\left(\frac{\partial c_p}{\partial n}\right)_w = \frac{2}{Re}\left[s_x\,\zeta_s + n_x\,\zeta_n\right]_w \quad . \tag{121}$$

Equation (121) may be used to eliminate $(\partial c_p/\partial n)_w$ from Eq. (120). The result is

$$\left(\frac{\partial c_p}{\partial s}\right)_w = -\frac{(n_x)_w}{Re\,\phi}\,(\zeta_s)_w - \frac{\phi}{Re\,(s_x)_w}\left[1 + \frac{(n_x)_w^2}{\phi^2}\right](\zeta_n)_w \quad . \tag{122}$$

From the Appendix, Eq. (12),

$$(n_x)_w = - \phi \, y_w' \quad ,$$

and, hence, using Eq. (13) of the Appendix,

$$1 + \frac{(n_x)_w^2}{\phi^2} = 1 + y_w'^2 = \alpha^2 \quad ,$$

From the Appendix, Eq. (9),

$$(s_x)_w = s_x = \alpha \quad .$$

Then, Eq. (112) may be written, using spline notation, as

$$\frac{Re}{2} \frac{dc_{p_w}}{ds} = y_w' \frac{d\zeta_w}{ds} - \phi \, \alpha \, \ell_w^{\zeta} \quad . \tag{123}$$

Equation (123) is now integrated between stations i-1 and i to yield

$$\frac{Re}{2}\left[\left(c_{p_w}\right)_i - \left(c_{p_w}\right)_{i-1}\right] = \int_{i-1}^{i} \left(y_w' \frac{d\zeta_w}{ds}\right) ds - \int_{i-1}^{i} \phi \, \alpha \, \ell_w^{\zeta} \, ds \quad .$$

The numerical evaluation of $d\zeta_w/ds$ can be avoided by integrating the first integral on the right-hand side by parts, thus:

$$\int_{i-1}^{i} \left(y_w' \frac{d\zeta_w}{ds}\right) ds = \left[y_w' \, \zeta_w\right]_{i-1}^{i} - \int_{i-1}^{i} \left(\frac{y_w''}{\alpha} \zeta_w\right) ds \quad .$$

Then the pressure coefficient relation becomes

$$c_{p_{w_i}} = c_{p_{w_{i-1}}} + \frac{2}{Re}\left[(y_w' \, \zeta_w)_i - (y_w' \, \zeta_w)_{i-1} - \int_{i-1}^{i} Q \, ds\right] \quad , \tag{124}$$

where

$$Q = \frac{y_w''}{\alpha}\,\zeta_w + \phi\,\alpha\,\ell_w^{\zeta} \quad . \tag{125}$$

The final result, obtained by evaluating the integral in Eq. (124) by the trapezoidal rule, is

$$c_{p_{w_i}} = c_{p_{w_{i-1}}} + \frac{2}{Re}\left[(y_w'\,\zeta_w)_i - (y_w'\,\zeta_w)_{i-1} - \left(\frac{Q_{i-1} + Q_i}{2}\right)(s_i - s_{i-i})\right] \quad . \tag{126}$$

III. RESULTS AND DISCUSSION

Problem Configurations

Numerical solutions are presented for six cases made up of five plate spacings and two Reynolds numbers (10^4 and 10^5). The parameters for each case are listed in Table 1. In cases 1-5, the rear plate is positioned below the front plate so that an adverse pressure gradient occurs on the connecting segment. In case 6, the situation is reversed and hence a favorable pressure gradient is produced. The choice of the number of grid lines in the streamwise (s) direction was guided by the work of Murphy [9], who solved a somewhat similar problem, and by the desire to keep the number of mesh points at a minimum so that run times would not be excessive. In Table 1, the guantities NX_I, NX_{II}, AND NX_{III} refer to the number of mesh intervals in regions I, II, and III, respectively.

In the present problem, Reynolds number has a somewhat arbitrary meaning because by rescaling the x and y coordinates, the Reynolds number is correspondingly rescaled as is the flow field since it is laminar. The important point to keep in mind is that the viscous layer must be properly resolved based on the boundary layer scaling.

Initial Profile Mesh Choice

As already mentioned, the initial conditions at $x = x_0$ consist of a Blasius boundary-layer profile adjacent to the wall and an outer uniform profile. A rapidly growing mesh in y is used which is small near the wall to properly resolve the boundary layer and is large in the outer region where flow gradients are negligible. This vertical grid point distribution, upon conversion from y to n, is then used for the entire computation region.

Table 1

Problem Parameters

CASE	1A	1B	2	3	4	5	6
Re	10^4	10^4	10^4	10^4	10^5	10^5	10^4
x_0	0.1	0.1	0.1	0.1	0.1	0.1	0.1
x_1	0.20129	0.20133	0.20059	0.20033	0.20033	0.20015	0.30116
x_2	0.30129	0.30133	0.30059	0.30033	0.30033	0.30015	0.40116
x_f	0.40259	0.40265	0.40119	0.40067	0.40065	0.40029	0.60231
y_{w_1}	0.10	0.10	0.10	0.10	0.10	0.10	0.10
y_{w_2}	0.085	0.085	0.090	0.0925	0.0925	0.095	0.11
y_e	0.20	0.20	0.20	0.20	0.125	0.125	0.20
NX_I	5	10	10	10	5	5	10
NX_{II}	5	10	10	10	5	5	5
NX_{III}	5	10	10	10	5	5	10
Δs	0.02026	0.01013	0.01006	0.01003	0.02007	0.02003	0.02012

The nodal distributions in zones 1 and 2 were generated by geometric progressions with different values of σ in each. In zone 1 the distribution of the Blasius similarity variable η was computed based on $\eta_\infty = 6$ and $\sigma = 1.1$ which gave ten intervals across the boundary layer. The present eleven-point spline solution gives $f''(0) = 0.46961$ compared to $f''(0) = 0.46960$ given in Table V.1 of Rosenhead [17]. From η_j the distribution of n_j at $x = x_0$ in zone 1 is computed using the relation

$$n_j = \frac{y_j - y_{w_1}}{y_e - y_{w_1}} \quad , \tag{127}$$

where

$$y_j = \left(\frac{2x_0}{Re}\right)^{1/2} \eta_j, \text{ for } 0 \leq \eta \leq 6 \quad . \tag{128}$$

In zone 2 the value of σ was computed because $y_e - \delta_0$ and the number of intervals (taken to be the same as in zone 1) were given. Thus, 21 points spanned the computational zone. A summary of the important initial profile grid parameters appears in Table 2 for the two Reynolds numbers used in this study. As can be seen, the values of σ_1 and σ_2 are nearly the same. When σ_2 was taken to be significantly different from σ_1, it was found that waviness appeared in the flow variables in the essentially inviscid outer region and no converged solution was obtained. The quantity n_{δ_0} in Table 1 is the value of n at the edge of the initial Blasius profile and indicates its thickness compared to the total computational zone thickness of unity.

Numerical Solution Procedure

The SLOR procedure was initialized by writing the starting profile, as a function of n, at all s-stations. Relaxation sweeps were performed in the positive s direction beginning at $s = s_0$ with two interior iterations of the Newton-Raphson procedure at each s-station. More interior iterations per profile were tried, but convergence of the entire flow field was not improved. In most cases, overrelaxation was performed on only ψ and ℓ^ψ, since they are principlly governed by the elliptic stream function equation. Above a relaxation factor of 1.2 the iterations diverged. Convergence of the solution was considered attained when

$$\max |\delta z_{i,j}| < \varepsilon$$

where z denotes the four-component column vector of unknowns defined by Eq. (54) and ε is a constant O(1).

25 January 1982
GHH:mmj

Table 2

Grid Parameters at Initial Station

Re	10^4	10^5
$y_e - y_{w_1}$	0.100	0.025
n_{δ_0}	0.26833	0.33941
σ_1	1.100	1.100
σ_2	1.110	1.039

Numerical Solutions

The numerical solutions presented in this report were run on the PSU IBM 370/3033 computer using double precision arithmetic. The two flow parameters presented from these numerical results are wall friction coefficient and wall pressure coefficient. The wall friction coefficient, c_f, is related to the wall vorticity by

$$c_f = -\frac{2}{Re}\zeta_w \quad .$$

The calculation of c_{p_w} has been described in Section II.

To determine the effect of convergence cutoff on the numerical solutions, case 1A was run for values of ε of 1.0, 0.1, and 0.01. The results, in terms of the effect on c_f, are presented in Table 3. The maximum change in c_f, going from ε of 1.0 to 0.01, is seen to be at most three in the fifth decimal place. Thus, $\varepsilon = 1.0$ was considered to be satisfactory for all cases. A cutoff of unity may seem unusually large until one realizes that the convergence test is dominated by $\ell\zeta$ whose maximum magnitude can be 10^3 or 10^4.

To gain a rough assessment of the effect of the horizontal mesh size on the solution, two values of Δs (one twice the other) were used to compute case 1 (cases 1A and 1B). The results for wall friction coefficient are shown in Fig. 3. The differences are largest in the unfavorable pressure gradient region just downstream of the end of the forward plate where $(\Delta c_f)_{max}$ is about 0.002 at x = 0.24. Other than the comparison of the initial Blasius solution with that of Rosenhead, no assessment has been made of the effect on the overall solution of changing the vertical mesh size Δn.

Overall run performance for the six cases (and sub-cases) is presented in Table 4. This table lists number of node points, iterations required for convergence, convergence cutoff and CPU time required. Cases 1B, 2, 3, and 6 had nearly twice the nodes in the s-direction as the other cases; hence, the run times are much higher. Run time can undoubtedly be reduced by careful reprogramming of the Blottner solver which in the present application recomputes all matrix coefficients at every mesh point for every internal (Newton-Raphson) and external (relaxation) iteration.

Cases 1, 4, and 5 all contain thin separated zones. No difficulties were encountered with convergence in case 1. To obtain convergence at the higher Reynolds number (10^5), especially in case 4, ζ and $\ell\zeta$ were under-related. The relaxation factors used were 0.5 in case 4 and 0.7 in case 5. The relaxation factor for ψ and $\ell\psi$ in these two cases was 1.0. A very long separated zone occurred in case 4 which extended beyond the downstream boundary. The extent of this separated zone is reflected in the larger number of iterations required for convergence, as shown in Table 4 (71 iterations for case 4 compared to 26 iterations for case 5). The stream-lines, including the separation streamline and the extent of the viscous

25 January 1982
GHH:mmj

Table 3

Effect of Convergence Cutoff on Wall Friction Coefficient, Case 1A

Sta	x	$\varepsilon = 1.0$	$\varepsilon = 0.1$	$\varepsilon = 0.01$
1	0.10000	.021002	.021002	.021002
2	0.12026	.021174	.021165	.021164
3	0.14052	.020821	.020808	.020807
4	0.16078	.020545	.020527	.020526
5	0.18104	.020842	.020820	.020817
6	0.20129	.023059	.023028	.023025
7	0.22149	.014322	.014294	.014291
8	0.24141	.003817	.003804	.003803
9	0.26118	-.000331	-.000337	-.000337
10	0.28110	-.001570	-.001573	-.001573
11	0.30129	-.001517	-.001522	-.001523
12	0.32155	-.000222	-.000233	-.000234
13	0.34181	.001290	.001275	.001274
14	0.36207	.002787	.002771	.002769
15	0.38233	.004161	.004147	.004145
16	0.40259	.005414	.005404	.005403

25 January 1982
GHH:mmj

Table 4

Run Performance

Case No.	Nodes M x N	Iterations To Converge	Cutoff (on ℓ^5)	CPU * Time (sec)
1A	16 x 21	27	1.0	138
1A	16 x 21	37	0.1	187
1A	16 x 21	47	0.01	237
1B	31 x 21	68	1.0	684
2	31 x 21	53	"	531
3	31 x 21	50	"	499
4	16 x 21	71	"	365
5	16 x 21	26	"	132
6	26 x 21	21	"	176

* IBM 370/3033

region (determined as $\zeta > 0.01$), are plotted in Fig. 4 for case 1 and Fig. 5 for case 4. These plots show that the viscous region covers about half the total computational zone.

Numerically calculated distributions for wall friction coefficient for all cases are shown in Figs. 6-11 and for wall pressure coefficient for cases 1, 2, 3, and 6 in Figs. 12-15. At the lower Reynolds number (10^4) comparisons are presented in Figs. 6-8 and 11-15 with potential flow-boundary layer solutions having no strong interaction coupling. These comparisons clearly show the extent and magnitude of the strong interaction effect. The potential flow-boundary layer solutions were obtained by a modification of the SFD parabolized vorticity code.

In cases 1, 2, and 3, where the rear plate is below the front plate, the flow first accelerates slightly as it approaches the convex center wall section and then abruptly slows down. This behavior is demonstrated by the wall pressure distribution, as shown in Figs. 12-14. The potential flow is seen to overpredict the levels of the favorable and unfavorable pressure gradients. Consequently, the peak in c_f, corresponding to the favorable pressure gradient, is much too high, as shown in Figs. 6-8. The magnitude of the potential flow adverse pressure gradient is so large that the boundary layer separates in all of these cases even though the parabolized vorticity solution separates (and reattaches) only in case 1, as shown in Fig. 6. The boundary-layer separation points in Figs. 6-8 are not the exact separation points, but the station where the boundary-layer calculation procedure failed to converge which indicates the procedure has marched across a separation point.

In case 6, where the rear plate is above the front plate, the boundary-layer solution separated just upstream of the beginning of the curved mid-section, as seen in the plot of c_f in Fig. 11. The reason for this behavior is shown in the wall pressure distribution, Fig. 15, where a strong adverse pressure gradient is predicted by the potential flow solution in that region. The flow is slowing down as it encounters the concave wall. The parabolized vorticity solution does not separate, however.

The wall pressure distributions, Figs. 12-15, clearly show that the large viscous region reduces the peaks and, hence, the magnitude of the gradients. Consequently, only in case 1 is the adverse pressure gradient strong enough to cause separation. With the strong interaction effects cutting down on the wall pressure peaks, the peaks in wall friction coefficient are also greatly reduced.

IV. CONCLUSIONS

For the present test geometry and Reynolds numbers the parabolized vorticity approximation, using a spline-finite difference discretization, is an efficient as well as effective way of treating the strong interaction problem. For attached flows, convergence of the SLOR procedure is rapid. The procedure

is also able to predict thin separated zones with acceptable convergence properties.

The results of this study reinforce the well-known observation that to obtain meaningful numerical results at high Reynolds numbers a viscous layer adjacent to a wall must be properly resolved according to the boundary-layer scaling. Proper resolution with a relatively sparse grid is achieved by use of fourth-order accurate splines to approximate flow quantities.

The effect of the slightly non-orthogonal coordinate system on the accuracy of parabolized vorticity model solutions will be dealt with in a future report.

REFERENCES

[1] Davis, R. T. and Rubin, S. G., "Non-Navier-Stokes Viscous Flow Computations," Computers and Fluids, 8, 101 (1980).

[2] Davis, R. T., "A Study of the Use of Optimal Coordinates in the Solution of the Navier-Stokes Equations," Rept. No. AFL 74-12-14, Dept. of Aerospace Engineering, University of Cincinnati, December 1974.

[3] Kaplun, S., "The Role of Coordinate Systems in Boundary Layer Theory," ZAMP, 5,111 (1954).

[4] Davis, R. T. and Rout, R. K., "Calculation of Optimal Coordinates for Two-Dimensional Incompressible Flow," Rept. No 79-7-47, Dept. of Aerospace Engineering and Applied Mechanics, University of Cincinnati, July 1979.

[5] Davis, R. T., "Numerical Solution of the Navier-Stokes Equations for Symmetric Laminar Incompressible Flow Past a Parabola," J. Fluid Mech., 51, 417 (1972).

[6] Ghia, U. and Davis, R. T., "Navier-Stokes Solutions for Flow Past a Class of Two-Dimensional Semi-Infinite Bodies," AIAA Journal, 12, 1659 (1974)

[7] Napolitano, M., Werle, M. J. and Davis, R. T., "Numerical Solutions for High Reynolds Number Separated Flow," Computers and Fluids, 7, 165 (1979).

[8] Steger, J. L., "Implicit Finite Difference Simulation of Flow About Arbitrary Two-Dimensional Geometries," AIAA Journal, 16, 679 (1978).

[9] Murphy, J. D., "An Efficient Numerical Method for the Solution of the Incompressible Navier-Stokes Equations," AIAA Journal, 15, 1307 (1977)

[10] Peaceman, D. W. and Rachford, H. H., Jr.," The Numerical Solution of Parabolic and Elliptic Differential Equations," Jour. Soc. Indust. Appl. Math., 3,28 (1955).

[11] Beam, R. M. and Warming, R. F., "Alternating Direction Implicit Methods for Parabolic Equations with a Mixed Derivative," SIAM J. Sci. Stat. Comput., 1, 131 (1980).

[12] Rubin, S. G. and Khosla, P. K., "Polynomial Interpolation Methods for Viscous Flow Calculations," Jour. Comp. Physics, 24, 217 (1977).

[13] Rubin, S. G. and Khosla, P. K., "Navier-Stokes Calculations with a Coupled Strongly Implicit Method, Part II: Spline Deferred-Corrector Solutions," in Approximation Methods for Navier-Stokes Problems, Proceedings of the IUTAM Symposium, Paderborn, Germany, September 1979, Springer-Verlag (1980), pp. 469-488.

[14] Keller, H. B., "Accurate Difference Methods for Nonlinear Two-Point Boundary Value Problems," SIAM J. Numer. Anal., 11, 305 (1974).

[15] Blottner, F. G., "Introduction to Computational Techniques for Boundary Layers," Sandia Laboratories Rept. SAND 79-0893, Albuquerque, N. M., September 1979.

[16] Chmielewski, G. E. and Hoffman, G. H., "Finite-Difference Solution of an Elliptic Partial Differential Equation with Discontinuous Coefficients," Internat. J. Numer. Meth. Engin., 12, 1407 (1978).

[17] Rosenhead, L., Ed., Laminar Boundary Layers, Oxford University Press (1963).

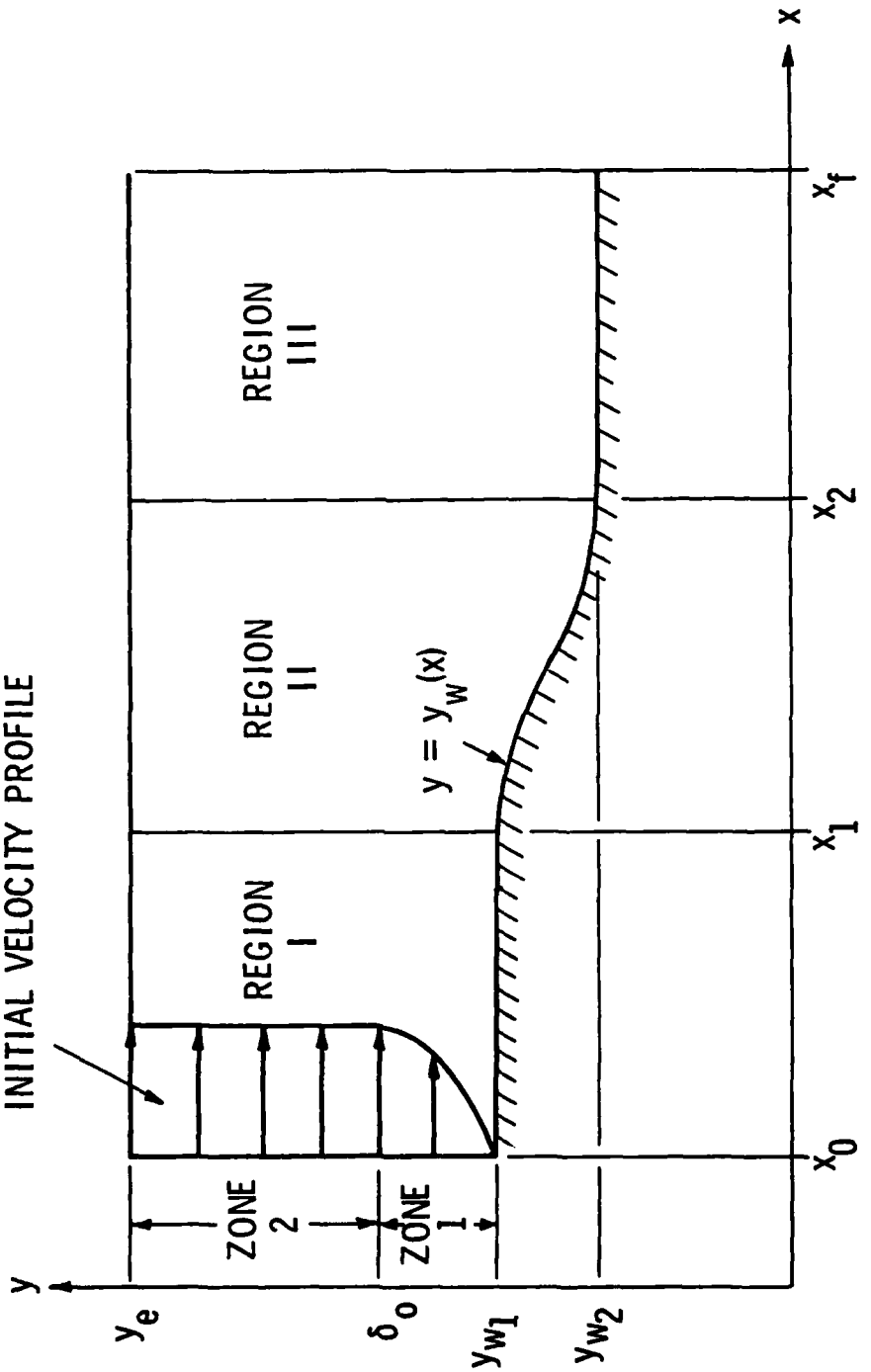

Fig. 1 Schematic of Computational Domain.

25 January 1982
GHH:mmj

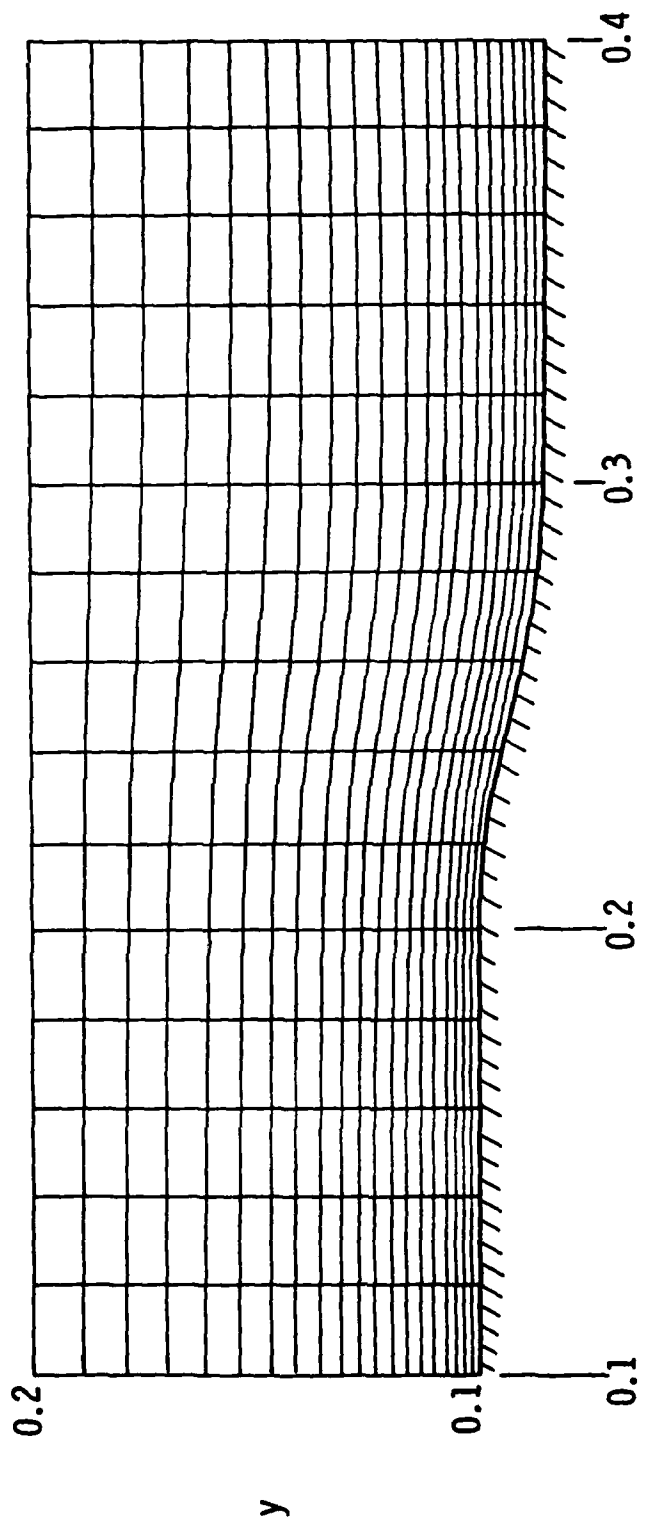

Fig. 2 Typical Sheared Grid.

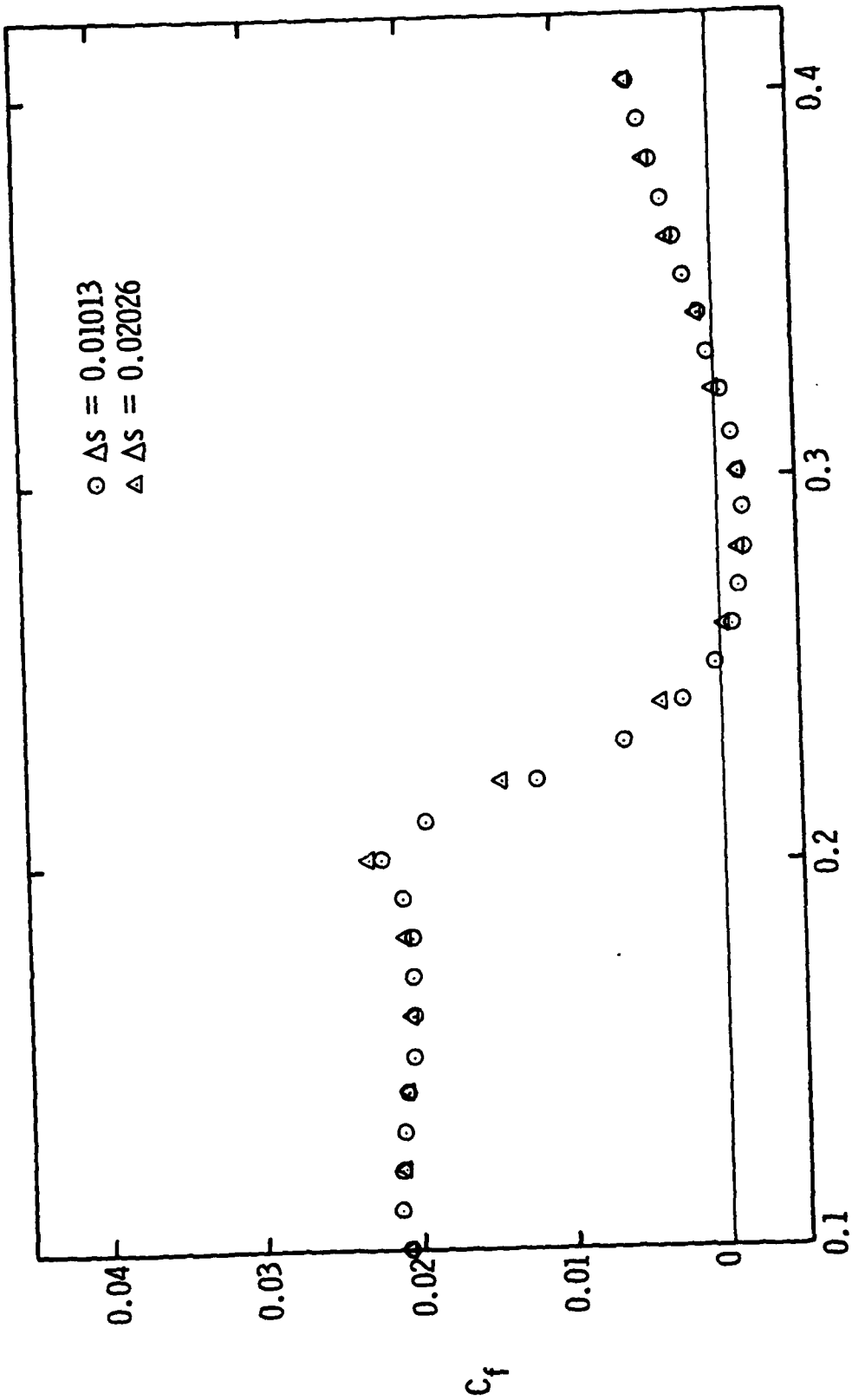

Fig. 3. Effect of Streamwise Stepsize on Wall Friction Coefficient, Case 1, Reynolds No. = 10^4.

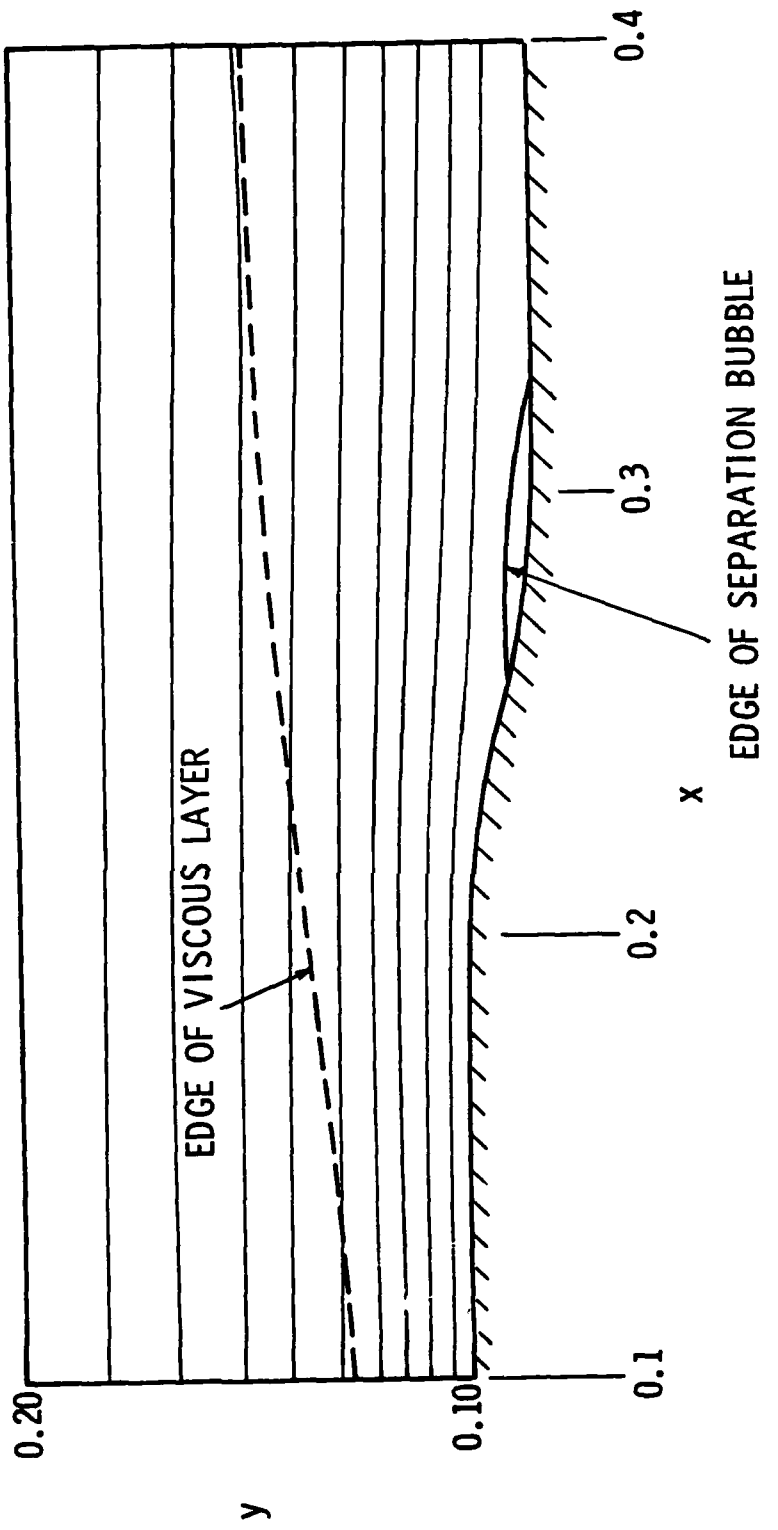

Fig. 4. Streamlines for Case 1, Re = 10^4.

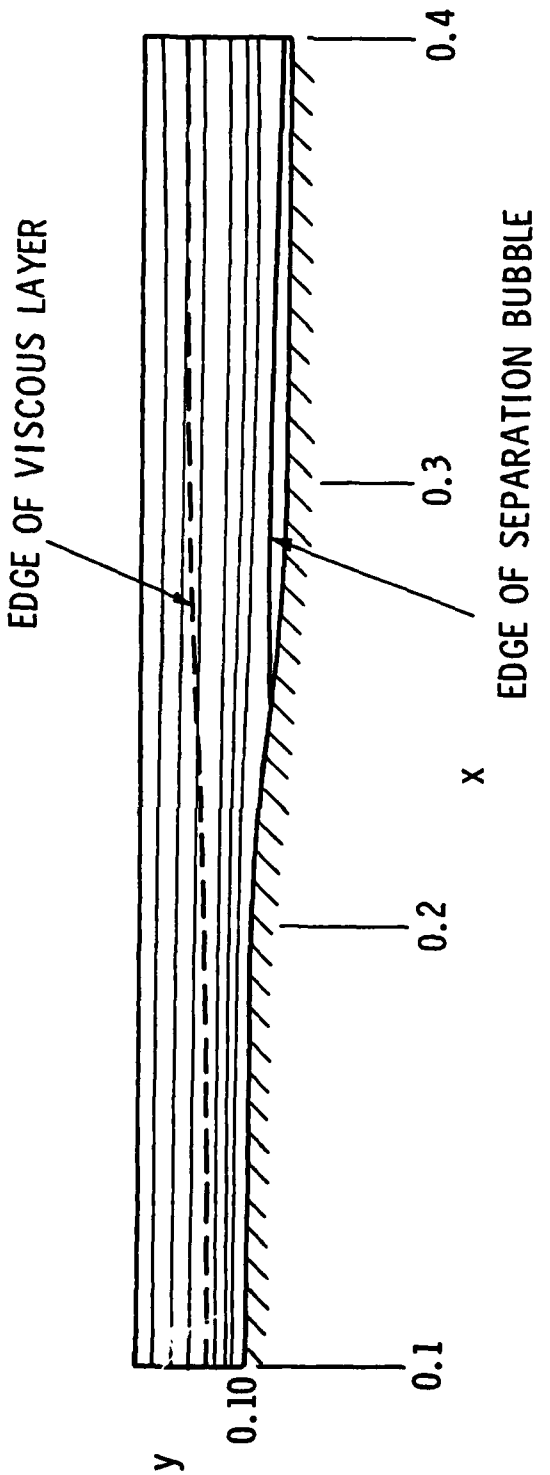

Fig. 5. Streamlines for Case 4, Re = 10^5.

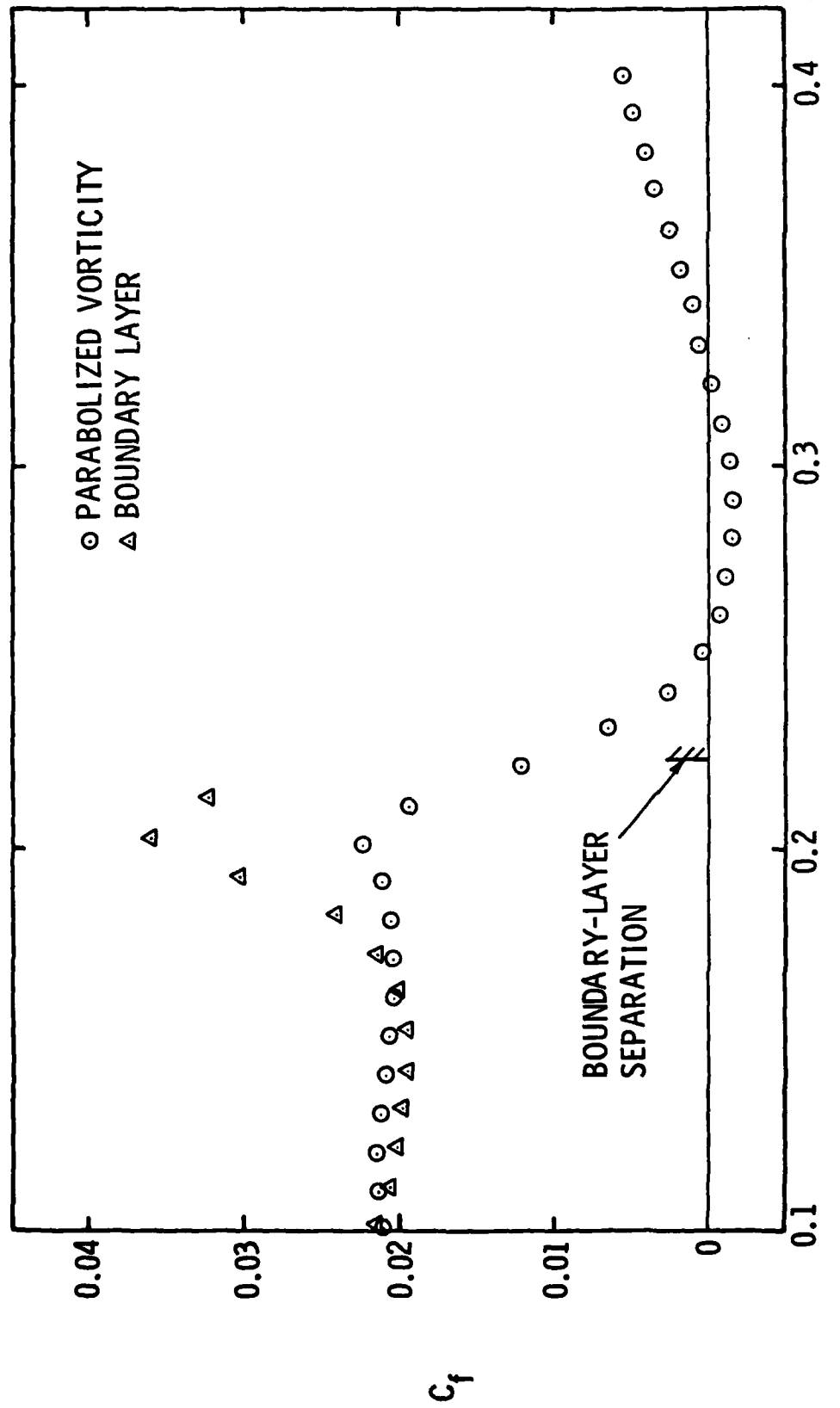

Fig. 6. Wall Friction Coefficient, Case 1B, Re = 10^4.

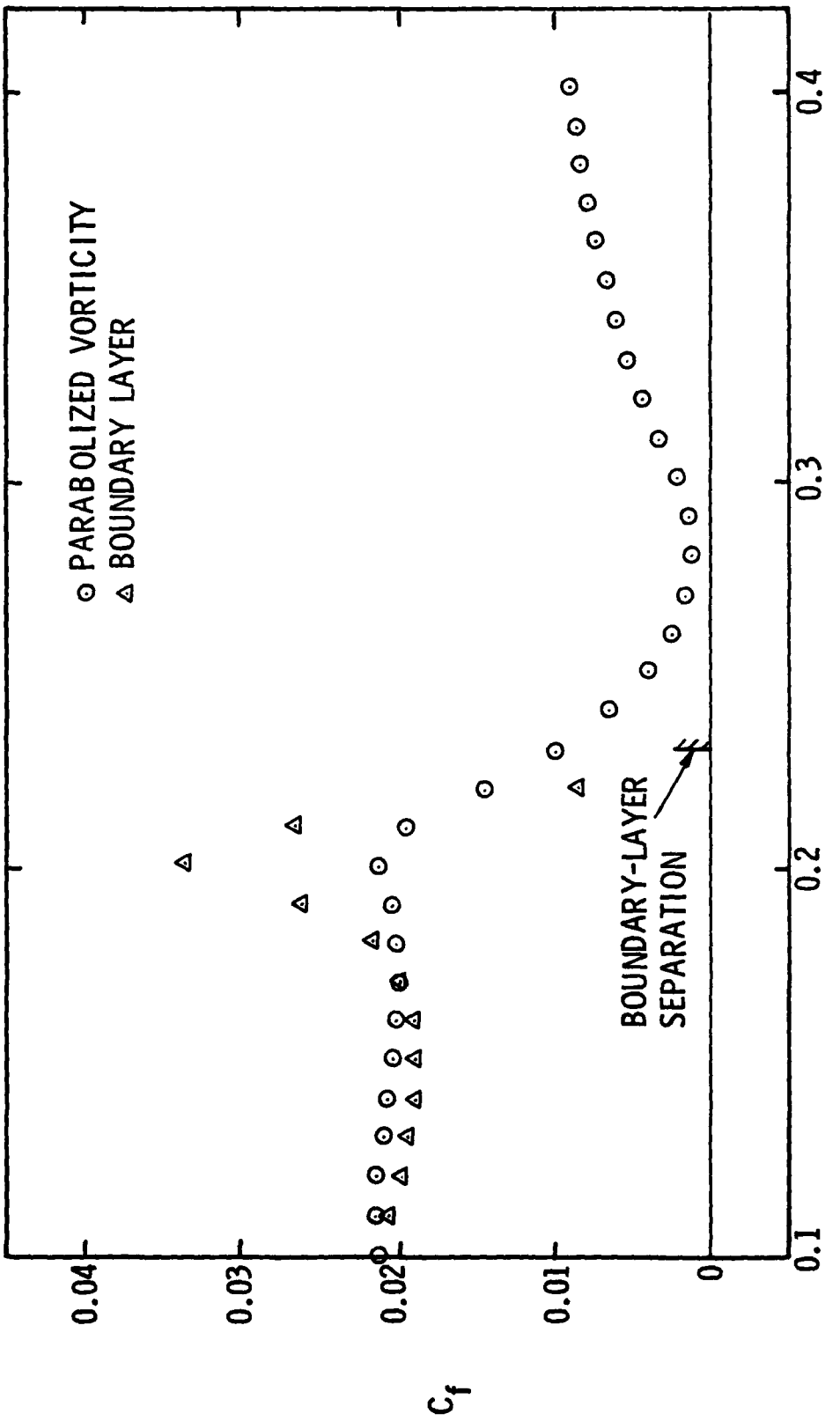

Fig. 7. Wall Friction Coefficient, Case 2, Re = 10^4.

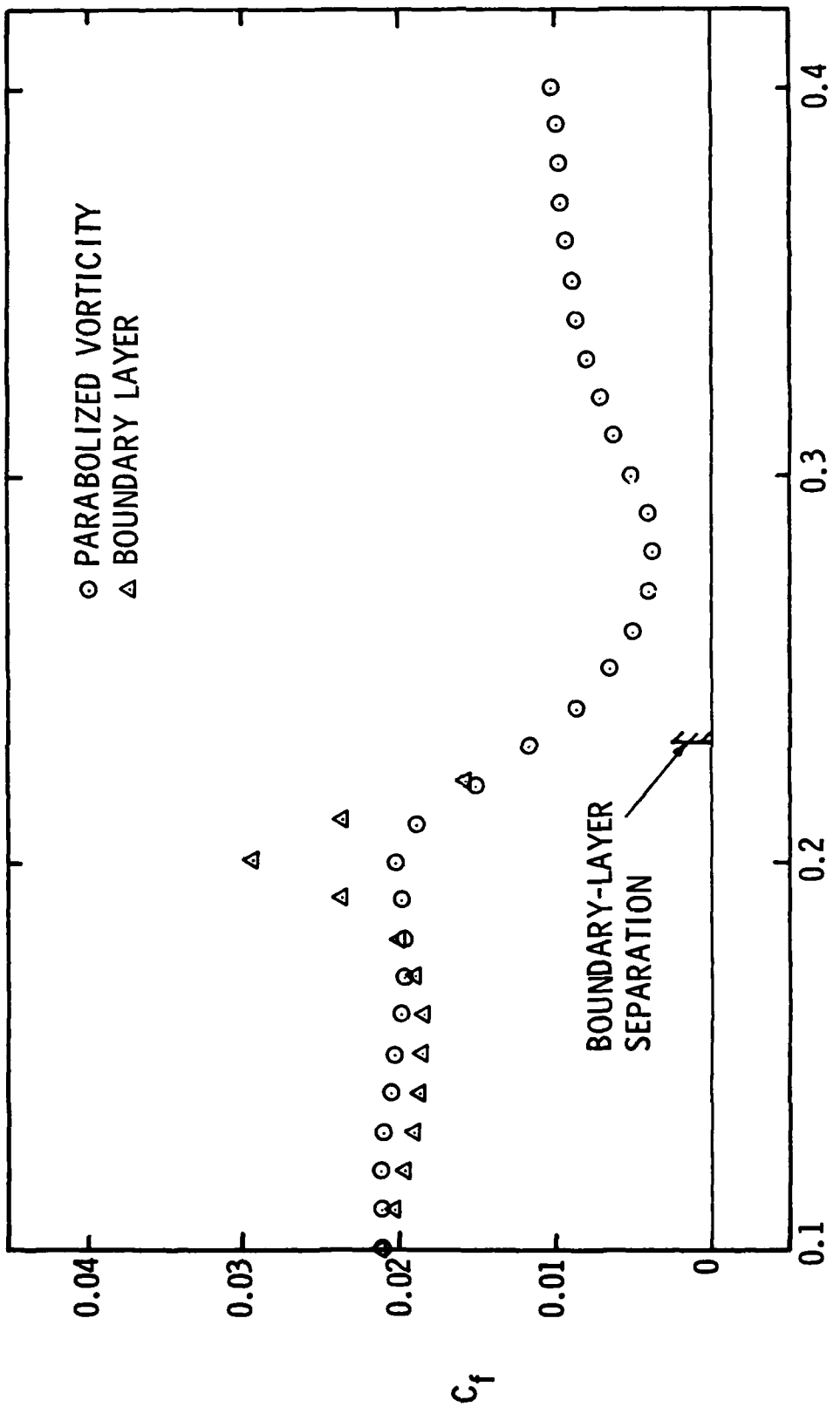

Fig. 8. Wall Friction Coefficient, Case 3, Re = 10^4.

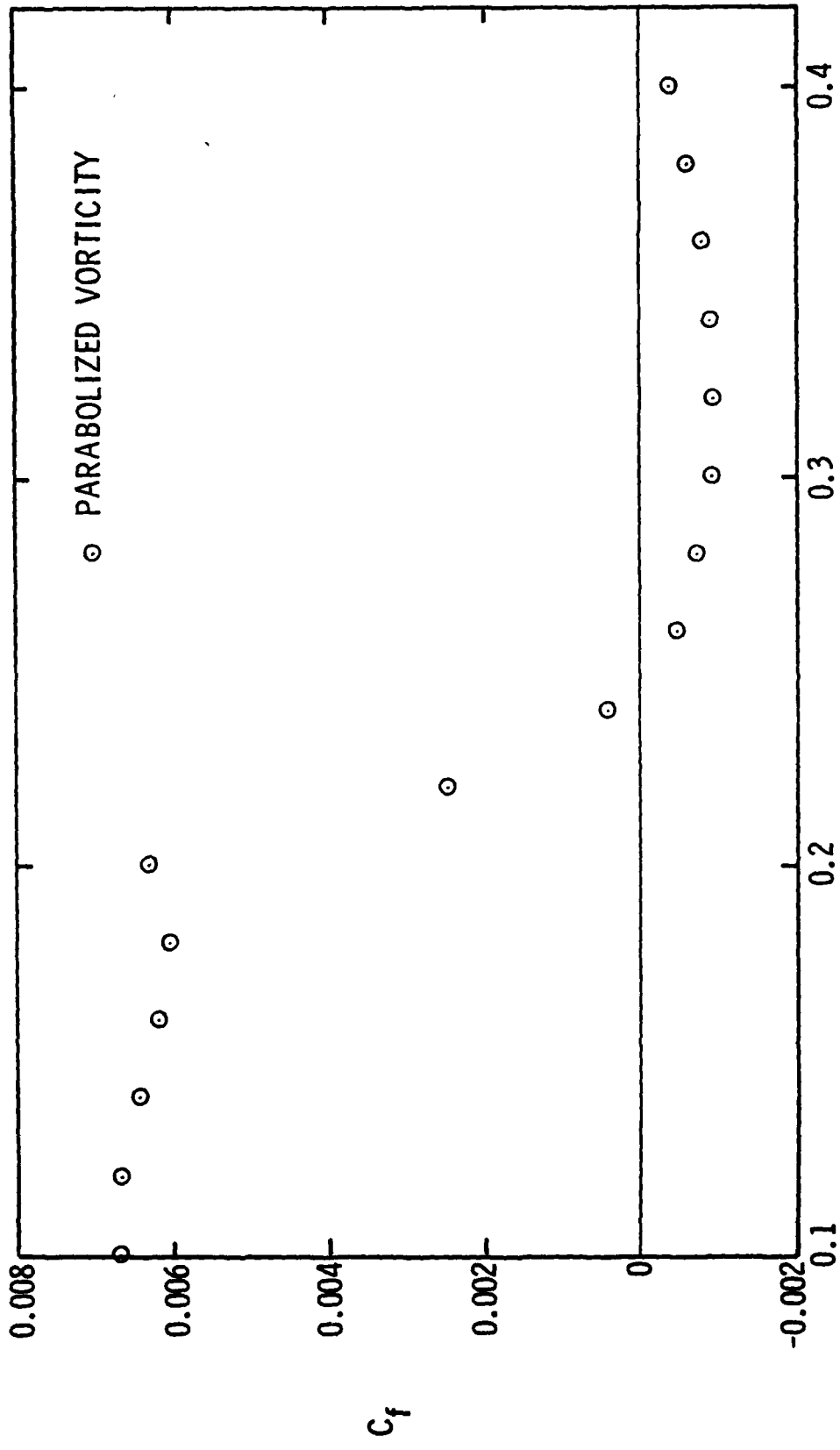

Fig. 9 Wall Friction Coefficient, Case 4, Re = 10^5.

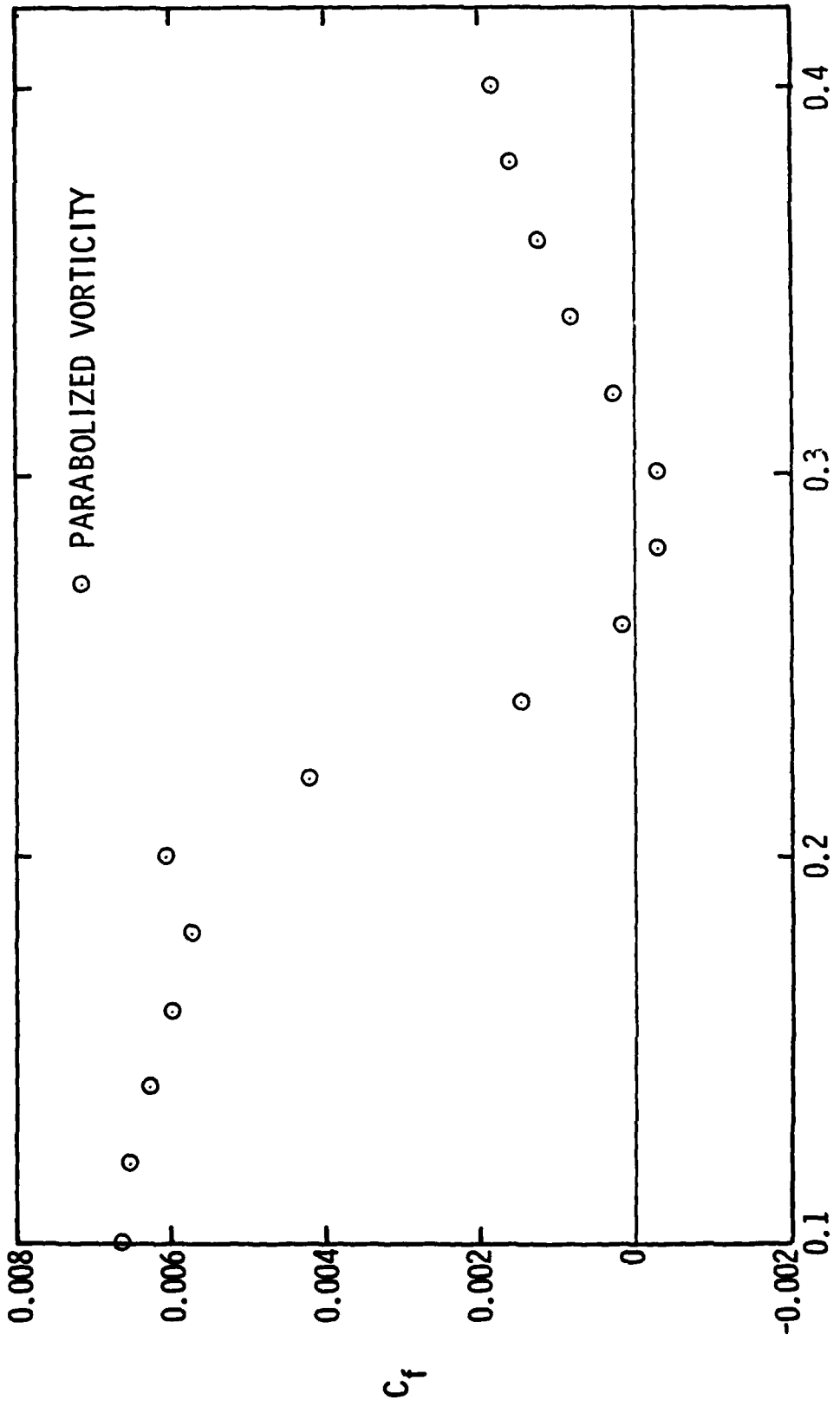

Fig. 10. Wall Friction Coefficient, Case 5, Re = 10^5.

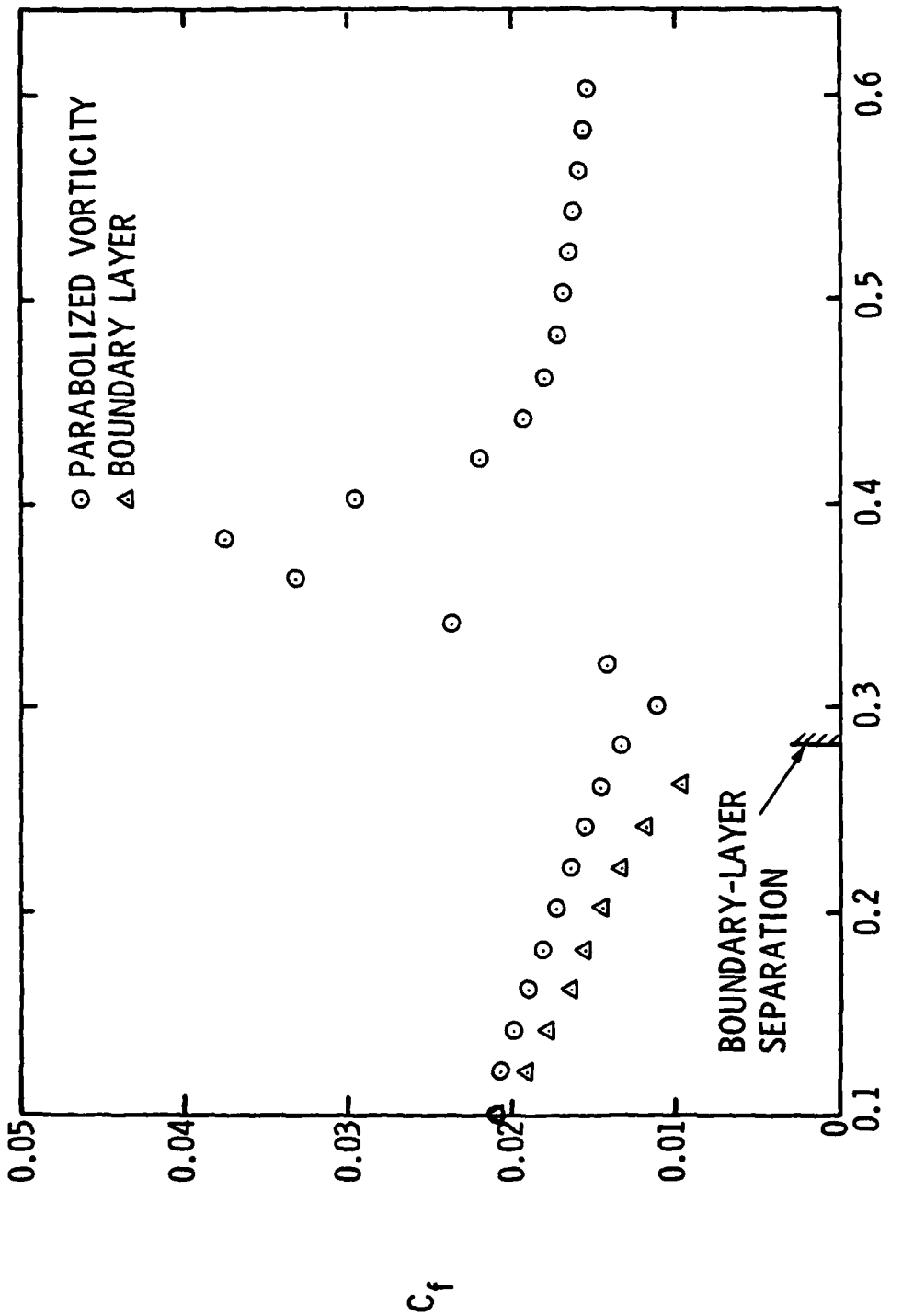

Fig. 11. Wall Friction Coefficient, Case 6, Re = 10^4.

25 January 1982
GHH:mmj

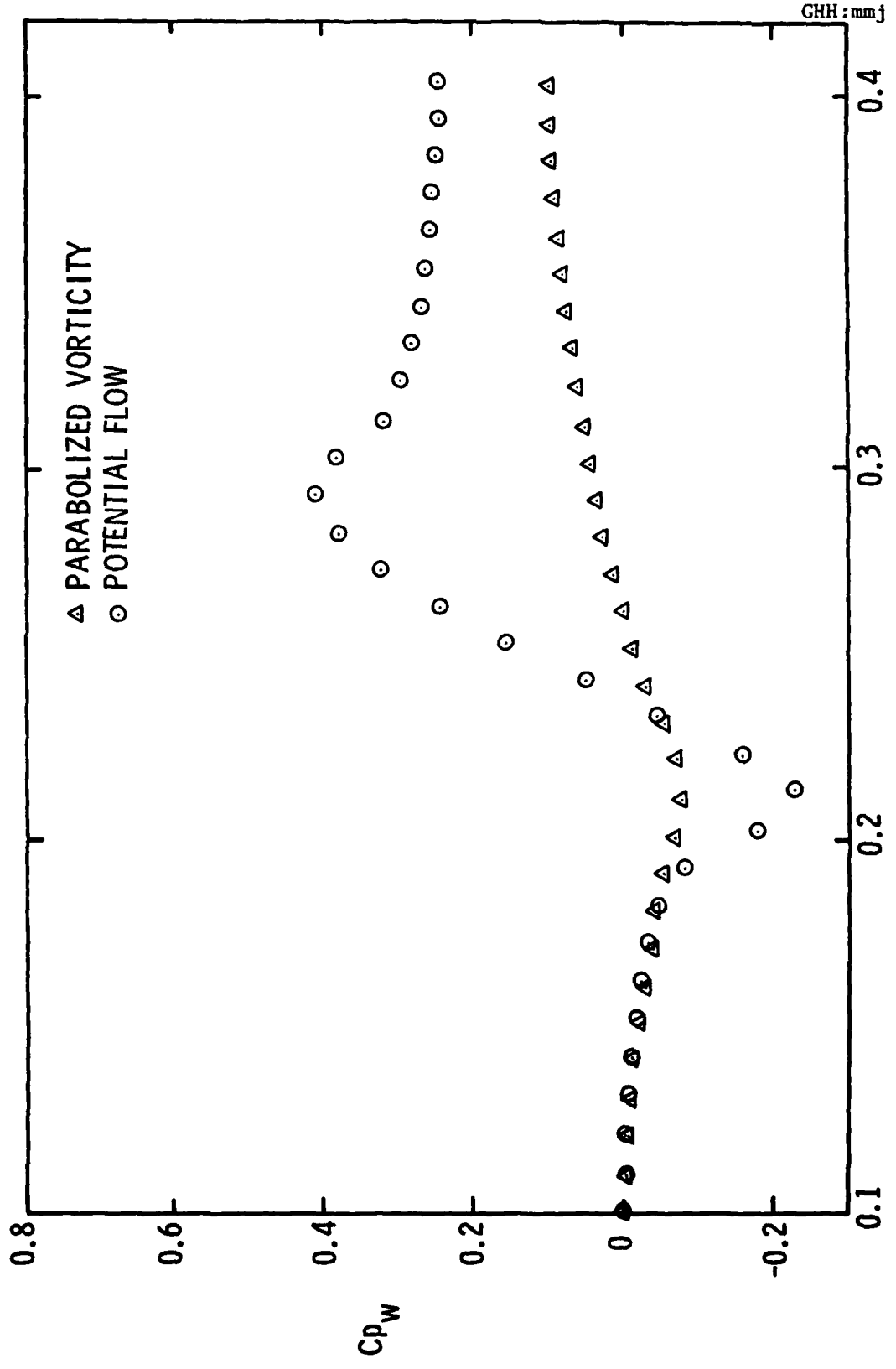

Fig. 12. Wall Pressure Coefficient, Case 1B, Re - 10^4.

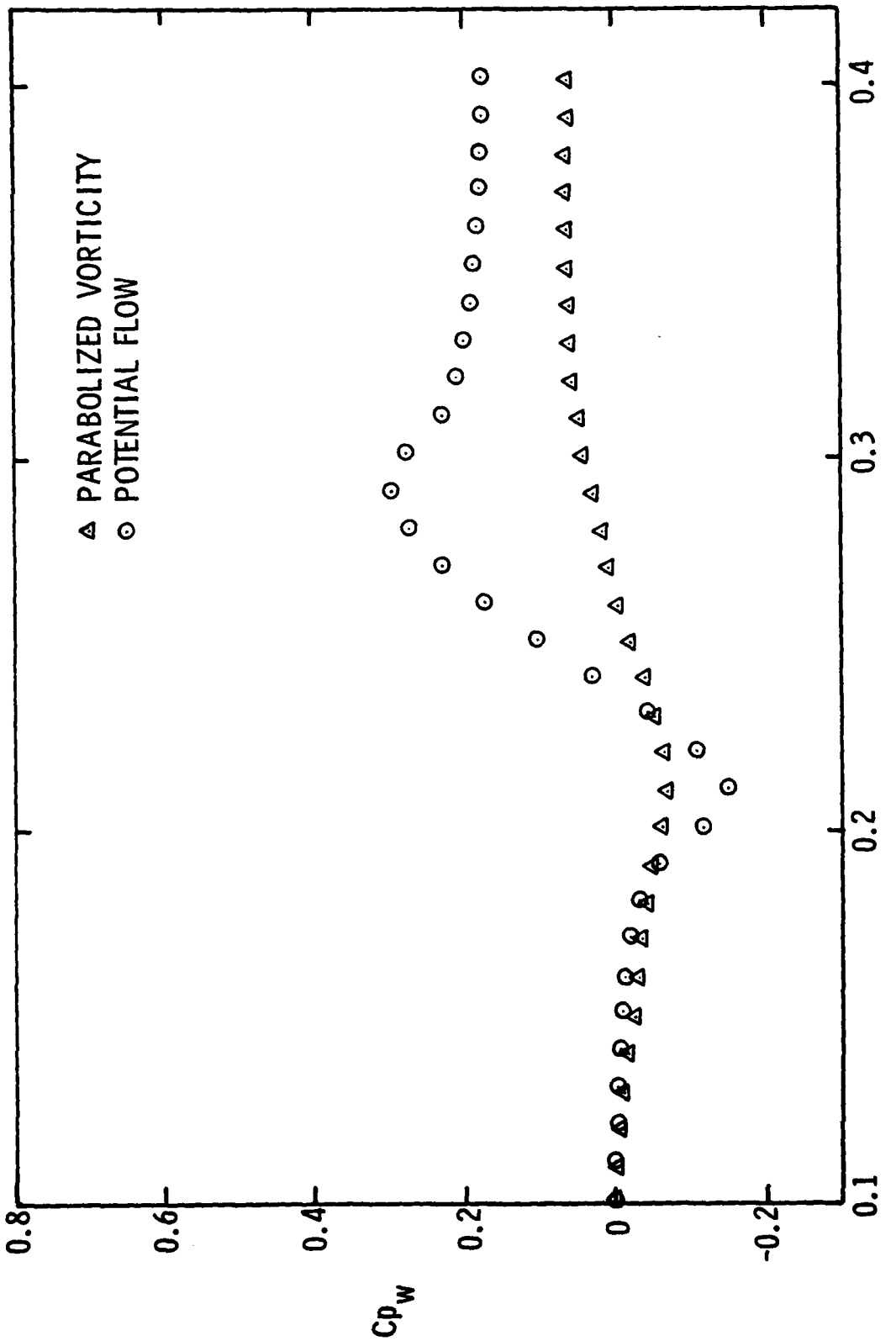

Fig. 13. Wall Pressure Coefficient, Case 2, Re = 10^4.

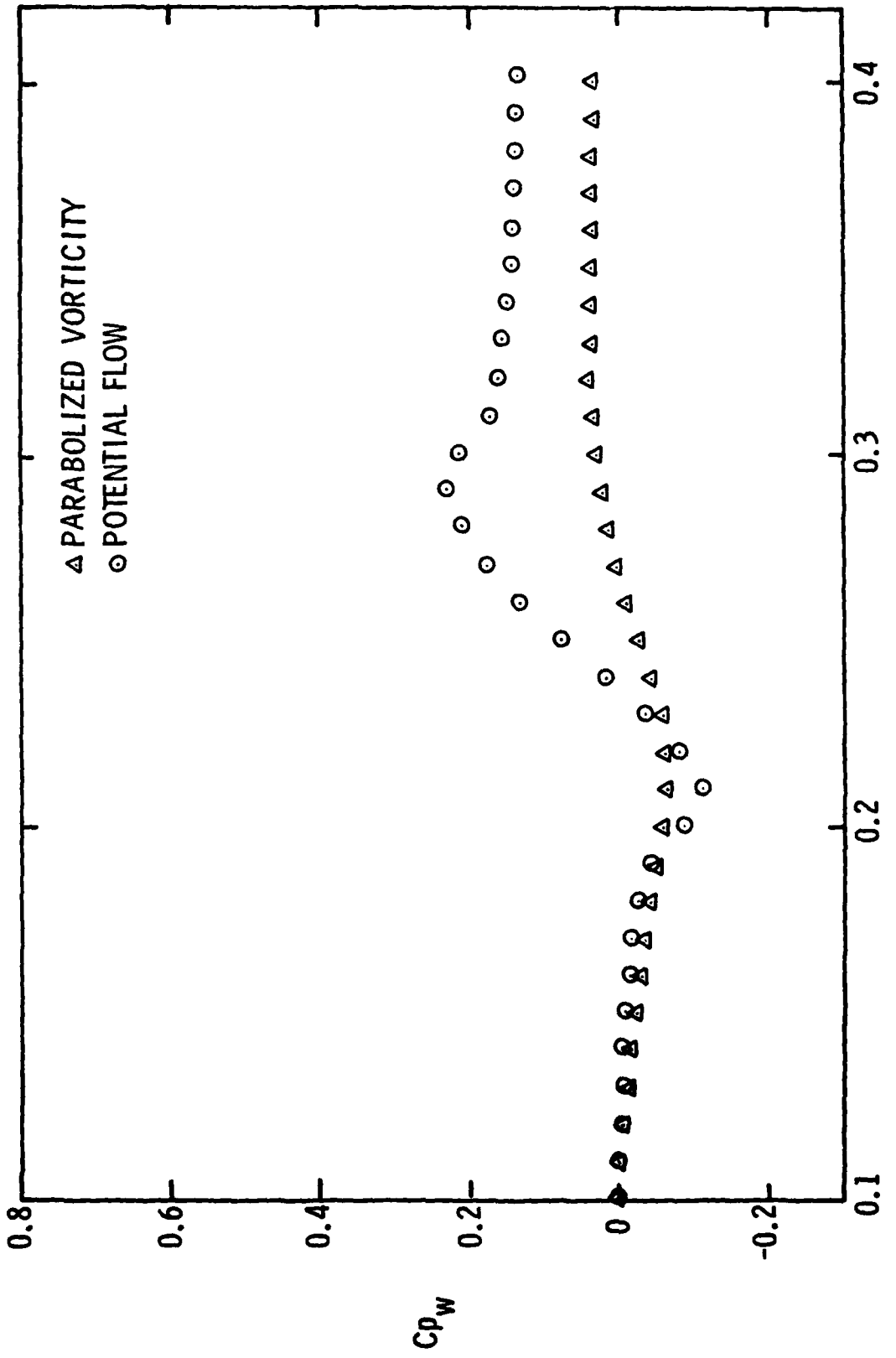

Fig. 14. Wall Pressure Coefficient, Case 3, Re = 10^4.

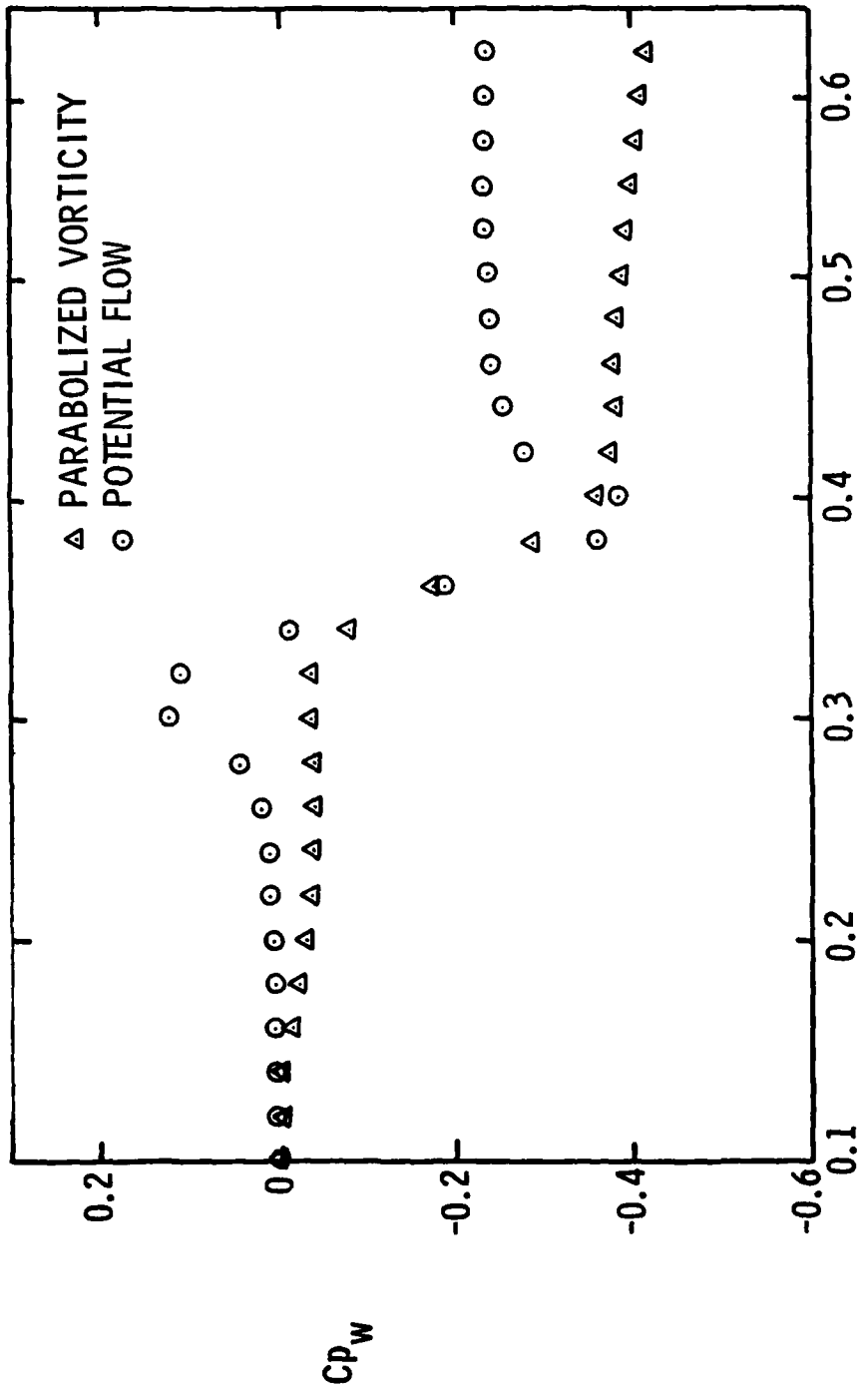

Fig. 15. Wall Pressure Coefficient, Case 6, Re = 10^4.

APPENDIX: METRIC COEFFICIENTS

The sheared coordinate transformation is

$$s = \int \alpha(x)\, dx \quad , \tag{A.1}$$

$$n = \phi(x) \cdot y - \lambda(x) \quad , \tag{A.2}$$

where

$$\alpha = (1 + y_w'^2)^{1/2} \quad , \tag{A.3}$$

$$\phi = \frac{1}{y_e - y_w} \quad , \tag{A.4}$$

$$\lambda = \frac{y_w}{y_e - y_w} \quad . \tag{A.5}$$

Thus, α, ϕ, and λ depend on the wall equation $y_w(x)$ and its derivative $y_w'(x)$. The wall equation is as follows: In regions I and III

$$y_w = \begin{cases} y_{w_1} \quad , & x_0 \leq x \leq x_1 \quad , \end{cases} \tag{A6a}$$

$$\begin{cases} y_{w_2} \quad , & x_2 \leq x \leq x_f \quad , \end{cases} \tag{A6.b}$$

while in region II, $y_w(x)$ is given by a cubic such that y_w and y_w' are continuous at the end points x_1 and x_2. The resulting equation is

$$y_w(x) = y_{w_1} + (w_2 - y_{w_1})\, \xi^2(3 - 2\xi) \quad , \tag{A.7}$$

where ξ is the normalized axial coordinate in region II, viz.

$$\xi = \frac{x - x_1}{x_2 - x_1} \quad . \tag{A.8}$$

Then the s-metric coefficients are, from Eq. (A.1):

$$s_x = \alpha \quad , \tag{A.9}$$

and

$$s_{xx} = \frac{y_w' \; y_w''}{\alpha} \tag{A.10}$$

From Eq. (A.2) the n-metric coefficients are:

$$n_y = \phi \quad , \tag{A.11}$$

and

$$n_x = \phi \; y_w' \cdot (n - 1) \quad , \tag{A.12}$$

and

$$n_{xx} = \phi(2\phi \; y_w'^2 + y_w'')(n - 1) \quad . \tag{A.13}$$

Examination of Eqs. (A.9) - (A.13) shows that only n_{xx} is discontinuous for the present case. A final observation is that $n_x = n_{xx} = 0$ on $n = 1$.

DISTRIBUTION LIST FOR UNCLASSIFIED TM 82-51 by G. H. Hoffman, dated 25 January 1982

Commander
Naval Sea Systems Command
Department of the Navy
Washington, DC 20362
Attn: T. E. Peirce
Code NSEA- 63R31
(Copy No. 1)

Commander
Naval Underwater Systems Center
Newport, RI 02840
Attn: D. Goodrich
Code 2634
(Copy No. 2)

Commander
David W. Taylor Naval Ship R&D Center
Department of the Navy
Bethesda, MD 20084
Attn: T. T. Huang
Code 1552
(Copy No. 3)

Commander
Naval Surface Weapons Center
Silver Spring, MD 20910
Attn: W. J. Glowacki
Code R-44
(Copy No. 4)

Office of Naval Research
Department of the Navy
Arlington, VA 22217
Attn: H. Fitzpatrick, Code 438
(Copy No. 5)

Office of Naval Research
Attn: A. H. Gilmore
(Copy No. 6)

Defense Technical Information Center
5010 Duke Street
Cameron Station
Alexandria, VA 22314
(Copy Nos. 7 through 12)

Naval Research Laboratory
Washington, DC 20390
Attn: Library
(Copy No. 13)

Superintendent (Code 1424)
Naval Post Graduate School
Monterey, CA 93940
(Copy No. 14)

NASA Lewis Research Center
21000 Brookpark Road
Cleveland, OH 44135
Attn: W. M. McNally
MS 5-9
(Copy No. 15)

Professor P. K. Khosla
Department of Aerospace Engineering and
Applied Mechanics
University of Cincinnati
Cincinnati, OH 45221
(Copy No. 16)

Professor C. L. Merkle
The Pennsylvania State University
Department of Mechanical Engineering
University Park, PA 16802
(Copy No. 17)

The Pennsylvania State University
APPLIED RESEARCH LABORATORY
P. O. Box 30
State College, PA 16801
Attn: R. E. Henderson
(Copy No. 18)

Applied Research Laboratory
Attn: S. A. Abdullah
(Copy No. 19)

Applied Research Laboratory
Attn: D. W. Prather
(Copy No. 20)

Applied Research Laboratory
Attn: C. G. Lauchle
(Copy No. 31)

Applied Research Laboratory
Attn: W. S. Gearhart
(Copy No. 32)

Applied Research Laboratory
Attn: M. R. Sheller
(Copy No. 33)

Applied Research Laboratory
Attn: G. H. Hoffman
(Copy No. 34)

Applied Research Laboratory
Attn: Garfield Thomas Water Tunnel Files
(Copy No. 35)

EN
DAT
FILME
4-8
DTI